JEM Journal of Experimental Medicine

ARTICLE

Multiple roles of lymphatic vessels in peripheral lymph node development

Esther Bovay[1], Amélie Sabine[1], Borja Prat-Luri[1], Sudong Kim[2], Kyungmin Son[2], Ann-Helen Willrodt[3], Cecilia Olsson[4], Cornelia Halin[3], Friedemann Kiefer[5,6], Christer Betsholtz[4,7], Noo Li Jeon[2], Sanjiv A. Luther[8], and Tatiana V. Petrova[1,9,10,11]

The mammalian lymphatic system consists of strategically located lymph nodes (LNs) embedded into a lymphatic vascular network. Mechanisms underlying development of this highly organized system are not fully understood. Using high-resolution imaging, we show that lymphoid tissue inducer (LTi) cells initially transmigrate from veins at LN development sites using gaps in venous mural coverage. This process is independent of lymphatic vasculature, but lymphatic vessels are indispensable for the transport of LTi cells that egress from blood capillaries elsewhere and serve as an essential LN expansion reservoir. At later stages, lymphatic collecting vessels ensure efficient LTi cell transport and formation of the LN capsule and subcapsular sinus. Perinodal lymphatics also promote local interstitial flow, which cooperates with lymphotoxin-β signaling to amplify stromal CXCL13 production and thereby promote LTi cell retention. Our data unify previous models of LN development by showing that lymphatics intervene at multiple points to assist LN expansion and identify a new role for mechanical forces in LN development.

Introduction

Lymphatic capillaries take up interstitial fluid, antigens, and antigen-presenting cells, and collecting vessels transport lymph to LNs. Afferent collecting lymphatics deliver lymph to the LN subcapsular sinus (SCS) through a fibrous capsule surrounding LNs. From the SCS, lymph reaches trabecular and medullary lymphatic sinuses and exits via the efferent collecting vessels. The LN and peripheral lymphatic endothelial cells (LECs) are molecularly distinct (Petrova and Koh, 2018). Such specialization is important for intranodal migration of dendritic cells (DCs; Ulvmar et al., 2014), filtration of small versus large molecular weight components (Rantakari et al., 2015), and immune tolerance (Cohen et al., 2010; Lund et al., 2012; Tewalt et al., 2012).

Mechanisms of how such a highly organized system arises during development are not fully understood. Pioneering studies have identified key roles for hematopoietic lymphoid tissue inducer (LTi) and stromal lymphoid tissue organizer (LTo) cells, proposing a model where LNs are initiated after CXCR5$^+$ pre-LTi cell egress to specific locations from blood vessels in response to LTo cell-derived CXCL13 (Ansel et al., 2000; Mebius et al., 2001; Yoshida et al., 2001; Luther et al., 2003; Ohl et al., 2003; van de Pavert et al., 2009; van de Pavert and Mebius, 2010; Brendolan and Caamaño, 2012). Clustering and crosstalk of LTαβ$^+$ LTi and LTβR$^+$ (lymphotoxin-β receptor) LTo cells result in further signal amplification, leading to LTi cell maturation and accumulation. Analysis of *Prox1*$^{-/-}$ embryos, which lack lymphatic vessels, revealed that most LNs are initiated in the absence of lymphatics, but their expansion is compromised (Vondenhoff et al., 2009b). Accordingly, *Vegfc*$^{+/-}$ embryos with defective lymphangiogenesis have small LNs (Lee and Koh, 2016). Recently, Onder et al. (2017) demonstrated that LEC-specific loss of LTβR and RANK impaired LN formation and proposed an alternative model, in which lymphatics initiate LNs by bringing disseminated LTi cells to the LN development site. The mechanism of LN capsule and SCS formation is also enigmatic. The SCS, the site of arrival of lymph and DCs, hosts resident phagocytes filtering pathogens and particles from the afferent lymph and is continuous with afferent collecting lymphatics. Currently, it is not known whether collecting lymphatic vessel development and maturation is linked to LN capsule and SCS formation.

[1]Department of Oncology, Centre Hospitalier Universitaire Vaudois and University of Lausanne, Epalinges, Switzerland; [2]School of Mechanical and Aerospace Engineering, Seoul National University, Seoul, Republic of Korea; [3]Institute of Pharmaceutical Sciences, ETH Zürich, Zürich, Switzerland; [4]Department of Immunology, Genetics and Pathology, Rudbeck Laboratory, Uppsala University, Uppsala, Sweden; [5]Max Planck Institute for Molecular Biomedicine, Münster, Germany; [6]European Institute for Molecular Imaging, University of Münster, Münster, Germany; [7]Integrated Cardio Metabolic Centre, Department of Medicine Huddinge, Karolinska Institute, Stockholm, Sweden; [8]Department of Biochemistry, University of Lausanne, Epalinges, Switzerland; [9]Ludwig Institute for Cancer Research, Epalinges, Switzerland; [10]Swiss Institute for Experimental Cancer Research, École Polytechnique Fédérale de Lausanne, Lausanne, Switzerland; [11]Division of Experimental Pathology, Centre Hospitalier Universitaire Vaudois, Lausanne, Switzerland.

Correspondence to Tatiana V. Petrova: tatiana.petrova@unil.ch.

© 2018 Bovay et al. This article is distributed under the terms of an Attribution–Noncommercial–Share Alike–No Mirror Sites license for the first six months after the publication date (see http://www.rupress.org/terms/). After six months it is available under a Creative Commons License (Attribution–Noncommercial–Share Alike 4.0 International license, as described at https://creativecommons.org/licenses/by-nc-sa/4.0/).

We propose that early LN development comprises both LTi cell egress from the veins, occurring independently of lymphatic vessels, and lymphatic transport of disseminated LTi cells to the LN site. We further show that efficient LTi cell transport, formation of the LN capsule, and specialization of the SCS at later embryonic stages require collecting lymphatic vessels. Perinodal lymphatics also promote local interstitial flow, which amplifies CXCL13 expression by LTo cells in cooperation with lymphotoxin-β signaling and thereby promotes LTi cell retention. Our data reveal a new role of mechanical forces in LN development and provide a unified model in which lymphatic vessels intervene at multiple points to assist LN expansion.

Results

Lymphatic vasculature remodeling at the site of LN development

Mouse embryonic lymphatic vessels first form a capillary-like plexus (Escobedo and Oliver, 2016), and at E15.5–E16.5, in response to increased lymph flow, part of this plexus matures into collecting vessels, characterized by low levels of LYVE1 and VEGFR3 and presence of intraluminal valves (Mäkinen et al., 2005; Norrmén et al., 2009; Sabine et al., 2012, 2015). We visualized remodeling of LN-associated lymphatic vessels using whole mount imaging of inguinal LNs (iLNs) at different stages of embryogenesis. At E15.5, as described earlier (Eberl et al., 2004; Vondenhoff et al., 2009b), single extravascular CD4$^+$ LTi cells and aggregates accumulated at bifurcations of the inguinal blood vessels, beneath the subepigastric vein/artery and above lymphatic vessels (Fig. 1, A and B). At E16.5, the lymphatic vessel beneath the LN anlage expanded and formed a shallow disk (Fig. 1 B). The disk progressively enlarged, forming a cup-like structure around growing CD4$^+$ LTi cell area, and almost fully engulfed it by E20–E20.5 (Fig. 1 B). While both peripheral and LN LECs express VEGFR3, NRP2 important for LEC sprouting (Xu et al., 2010) was detected only on peripheral LECs. The NRP2 was low in the lymphatic cup around LN anlage and was expressed only in few sprouting LECs at the cup edge (Fig. 1, C and D). 20% of LECs proliferated in the lower part of the cup, and this proportion increased to 30% in the upper part (Fig. 1, E, E′, and F). Lymphatic vessel expansion around the LN anlage is thus a process distinct from lymphatic vessel growth occurring in skin. In the former case, we observed a coordinated extension of continuous double LEC layers, which eventually engulfs the LN anlage. In contrast, peripheral lymphatic vessels display multiple sprouts and form a mesh-like network (Fig. 1 G).

Extracellular matrix and smooth muscle cells (SMCs) surround embryonic LNs

At E18.5, SMCs were associated with the exterior LN LECs and closely followed the expanding LEC sheet (Fig. 2, A and A′), indicating coordinated formation of the LN capsule. Staining for collagen IV revealed increased extracellular matrix deposition around the LN capsule (Fig. 2 B). PDGFβ, a growth factor essential for vascular SMC recruitment (Wang et al., 2017), was expressed by the outer LEC layer (Fig. 2 C). Taken together, our data demonstrate that the growing LN induces a coordinated remodeling and expansion of adjacent lymphatic vessels. As a result, the newly formed lymphatic cup envelops the developing LN while maintaining overall vessel integrity and function (Fig. 2 D).

LN initiation and early expansion require both blood and lymphatic vessels

Earlier models proposed that LNs are formed by RORγt$^+$ CD4$^-$ CXCR5$^+$ pre-LTi cells exiting from blood vessels in response to CXCL13 produced by fibroblastic LTo cells (van de Pavert et al., 2009, 2014). Onder et al. (2017) suggested that lymphatic vessels initiate LN formation by transporting LTi cells to the LN site and by increasing LTi cell retention through CCL21$^+$ perinodal lymphatics. To characterize the LN initiation process in more detail we first visualized the localization of CD4$^+$ LTi cells and blood vessels at different development stages by staining for αSMA (α-smooth muscle actin), the venous marker endomucin, and the basement membrane component laminin α5. We observed significantly higher SMC coverage of the subepigastric vein at the iLN site at E16.5 in comparison to E15.0 (Fig. 3, A–C). At E15.0, only arteries produced laminin α5, which inhibits the T cell egress from blood vessels (Wu et al., 2009; Fig. 3 B). We also observed a strikingly different SMC coverage of the subepigastric vein along the anterior–posterior axis: the vein in the axillary region had a continuous SMC layer, but SMCs at the venous bifurcation in the iLN area were so sparse that it was difficult to detect the vein contour (Fig. 3, C–E). In contrast, we observed high laminin α5 deposition and complete venous SMC coverage in both locations after E16.5 (Fig. 3, B and C). Importantly, at E15, we observed LTi cell trafficking in SMC-low gaps in the venous EC layer (Fig. 3, F and F′). Significantly, we did not observe CD4$^+$ LTi cells in the venous lumen. Because CD4 marks mature LTi cells (van de Pavert et al., 2009, 2014), we analyzed E15.0 *Rorc*(γt)$^{EGFP/+}$ embryos, in which both RORγt$^+$ CD4$^-$ pre-LTi and mature RORγt$^+$ CD4$^+$ LTi cells can be observed. Indeed, only a proportion of extravascular iLN RORγt$^+$ cells was CD4$^+$ (Fig. S1, A and B). Most importantly, we observed intravenous RORγt$^+$ cells in the iLN area in close contact with ECs (Fig. S1, C and C′). These results are consistent with the model in which immature RORγt$^+$ CD4$^-$ LTi cells egress from the vein and undergo further extravascular maturation.

To study if LTi cell transmigration alters venous SMC coverage, we analyzed *Id2*-deficient embryos, which lack LTi cells (Fig. S1, D–F; Yokota et al., 1999; Rawlins et al., 2009). Venous SMC coverage was still reduced in the iLN regions in these mice (Fig. S1, D–F); therefore, low SMC coverage is an intrinsic characteristic of the vein at this location at E15. Finally, we analyzed *Pdgfb*$^{ret/ret}$ embryos, which have low perivascular Pdgfβ and reduced recruitment of mural cells to blood vessels (Lindblom et al., 2003). The iLNs were significantly bigger in *Pdgfb*$^{ret/ret}$ embryos in comparison to the controls, indicating that SMC coverage of blood vessels is an important factor regulating LN development (Fig. 3, G and H). These results support the notion that during LN initiation, pre-LTi cells egress at LN development sites using gaps in venous mural coverage and then undergo further local maturation.

To study whether lymphatic vasculature is necessary for pre-LTi cell egress from the vein, we blocked lymphangiogenesis by administering VEGFR3-blocking antibodies. In agreement with

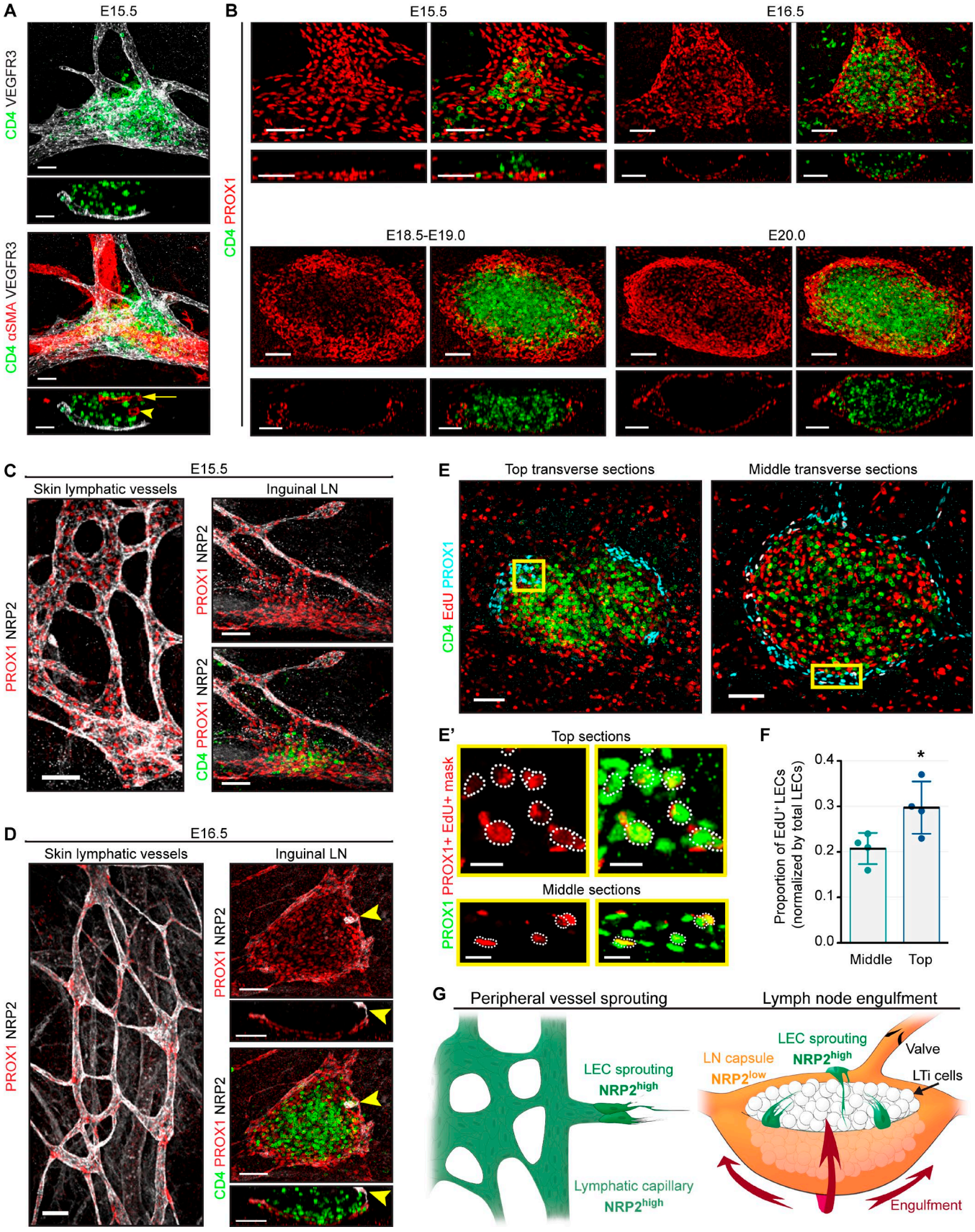

Figure 1. **Lymphatic vessel remodeling during LN development. (A)** LTi cells accumulate between lymphatic vessels and the subepigastric vein. Whole mount and frontal view (10 µm) of iLN: CD4 (green), VEGFR3 (white), and αSMA (red). Arrowhead indicates artery; arrow indicates vein. E15.5, *n* = 6. Scale bar, 50 µm. **(B)** Lymphatic remodeling during iLN development. Whole mount and frontal views (10 µm): PROX1 (red) and CD4 (green). E15.5, *n* = 4; E16.5, *n* = 5;

Zheng et al. (2014), the treatment severely diminished dermal lymphatics (Fig. 3 I). However, prominent, albeit reduced LTi cell accumulation was still observed in LN anlagen in the absence of associated lymphatic vessels (Fig. 3 I; LN volume, 10^3 µm^3; control IgG, 319.2 ± 115.9; VEGFR3-blocking IgG, 79.2 ± 25.5; P = 0.0272). Furthermore, we readily visualized LTi cells in SMC-low gaps in the vein in both control and VEGFR3 IgG-treated embryos (Fig. 3 I′).

We next monitored the global distribution of CD4$^+$ LTi cells in the embryonic skin. We observed CD4$^+$ cells associated with the upper dermis blood vascular plexus (Fig. 3, J and J′). Isolated CD4$^+$ cells and clusters were frequently present in the lymphatic plexus at E15.5 and later in lymphatic capillaries and in afferent and efferent LN collecting vessels (Fig. 3, K and L; and Fig. S2, A–D). A similar distribution of GFP$^+$ cells was observed in *Rorc*(γt)$^{EGFP/+}$ embryos (Fig. S2, E–G). Our data corroborate lymphatic vessel–independent LN initiation model also for the iLN (Vondenhoff et al., 2009b). However, in agreement with Onder et al. (2017), they show that a reservoir of disseminated LTi cells critically contributes to LN expansion. These results unify the previous models and further suggest that the SMC coverage in part defines the site and the time of pre-LTi cell egress from veins.

Efficient LTi cell uptake and transport to the LN anlagen requires CCR7 signaling

Following VEGFR3 blockade, we sometimes observed isolated LEC spheroids (Fig. 4 A), likely formed by nonvenous dermal LEC progenitors (Martinez-Corral et al., 2015). The LEC spheroids contained CD4$^+$ cells (Fig. 4 B), indicating that even disconnected LECs attract LTi cells. In adults, CCR7 drives migration of DCs and T cells toward and inside of CCL21$^+$ initial lymphatics (Ohl et al., 2004; Bromley et al., 2005; Debes et al., 2005; Russo et al., 2016). Because LTi cells express functional CCR7 (Honda et al., 2001), we analyzed iLN development in *Ccr7*$^{-/-}$ mice. While the lymphatic vascular development was not affected (Fig. S2, H and I), *Ccr7*$^{-/-}$ iLNs were smaller, and we observed almost no intralymphatic LTi cell clusters (Fig. 4, C–E). Meanwhile, the extravascular CD4$^+$ LTi cell fraction was increased (Fig. 4 F). Therefore, in addition to the role of CCL21 in LTi cell retention at LN site (Onder et al., 2017), CCL21$^+$ initial lymphatics attract and collect disseminated LTi cells.

Loss of CXCR5 leads to tissue and intralymphatic accumulation of LTi cells

In addition to CD4$^+$ cells in lymphatic capillaries and afferent LN lymphatics, we observed a low but significant number of CD4$^+$ cells in iLN efferent vessels (Fig. S2, A and D). The dynamic equilibrium between arriving, retained, and departing LTi cells thus defines the iLN size. To study whether defective retention of LTi cells shifts the balance toward LTi cell accumulation in lymphatic vessels, we analyzed *Cxcr5*$^{-/-}$ embryos. Loss of CXCR5$^+$ LTi cell attraction by CXCL13$^+$ LTo cells prevents formation of most peripheral LNs, including iLN (Förster et al., 1996; Ansel et al., 2000; Ohl et al., 2003; Fig. 4, G, G′, and H). Lymphatic vessels at the presumptive *Cxcr5*$^{-/-}$ iLN site did not develop the characteristic lymphatic cup found in WT mice but maintained a collecting vessel phenotype (Fig. 4, G and G′). As in *Cxcr5*$^{-/-}$ animals, lymphatic vessel remodeling into a LN capsule was abolished in *LTb*$^{-/-}$ embryos (Koni et al., 1997), which do not form peripheral LNs due to lack of surface LTβ presentation (Fig. S2, J and K), further confirming the driving role of LN anlagen in LN capsule and SCS development. Strikingly, lymphatic vessels of *Cxcr5*$^{-/-}$ mice were filled with intralymphatic CD4$^+$ clusters (Fig. 4 I and Fig. S2 L). Such clusters were biggest at the presumptive iLN site, but smaller clusters were also disseminated throughout the lymphatic vascular network (Fig. 4 I). Furthermore, the number of isolated CD4$^+$ cell in the skin interstitium was increased (Fig. 4 J). Our results thus show that extravascular LTi cell accumulation is a prerequisite for the induction of lymphatic vessel remodeling and LN capsule formation.

SCS specialization occurs prenatally and coincides with lymphatic vascular maturation

Acquisition of a capillary or collecting phenotype is a key step of lymphatic vascular development. In skin, this process starts at E15.5–E16.5 and thus coincides with initiation of iLN capsule formation. We studied whether all LECs of the LN lymphatic cup belong to one or another vessel type by staining for collecting or capillary markers FOXC2 or LYVE1 (Schulte-Merker et al., 2011). The LECs of the outer layer expressed high levels of FOXC2, whereas LECs in the inner layer were FOXC2$^-$ but produced higher levels of LYVE1 (Fig. 5 A), indicating a hybrid collecting–capillary identity of the prenatal SCS.

Such organization is reminiscent of adult LN SCS, which contains distinct populations of ceiling LECs (cLECs) and floor LECs (fLECs). Only cLECs produce the chemokine receptor CCRL1, while fLECs express LYVE1, ITGA2B, and MadCAM1 (Cohen et al., 2010; Ulvmar et al., 2014; Cordeiro et al., 2016). In adult LNs of *Ccrl1*-EGFP mice, FOXC2 was coexpressed with CCRL1 in cLECs (Fig. S3, A and A′), confirming conservation of asymmetric FOXC2 localization within the SCS. In embryonic iLNs, the inner LECs expressed fLEC-specific ITGA2B and MadCAM1, whereas a subset of outer LECs produced CCRL1 (Fig. 5, B–D). We observed continuous CCRL1 expression in cLECs in axillary LN, more advanced in its development (Fig. 5 D; Rennert et al., 1996). The VEGFR3$^+$ collagen IV$^+$ LECs interconnected the cLEC and fLEC layers (Fig. 5 E). Such pillars were LN specific and were absent in all other lymphatic vessels examined. They likely

E18.5–E19.0, *n* = 6; E20.0, *n* = 3. Scale bar, 50 µm. **(C)** Peripheral but not LN LECs express NRP2. Whole mount skin: NRP2 (white), PROX1 (red), and CD4 (green). E15.5, *n* = 4. Scale bar, 50 µm. **(D)** LECs at the LN sprouting edge express NRP2. Whole mount and frontal view (10 µm): NRP2 (white), PROX1 (red), and CD4 (green). Arrowheads indicate NRP2$^+$ LECs. E16.5, *n* = 6. Scale bar, 50 µm. **(E)** LN LECs actively proliferate. Whole mount views in the top (20 µm) and middle (5 µm) iLN areas: CD4 (green), PROX1 (blue), and EdU (red). E18.5, *n* = 4. Scale bar, 80 µm. **(E′)** High-magnification view of the yellow box in E. A mask was applied to identify EdU$^+$ PROX1$^+$ cells (red). Dotted line indicates PROX1$^+$ EdU$^+$ nuclei. Scale bar, 20 µm. **(F)** Quantification of EdU$^+$ LECs in the top and middle parts of the LN cup. E18.5, *n* = 4. Two-tailed unpaired Student's *t* test; *, P < 0.05. Data are shown as mean ± SD. **(G)** LEC sprouting versus LN engulfment. All peripheral LECs express NRP2 (NRP2^{high}), but only few LECs at the borders of converging double-walled LN LEC layer are NRP2$^+$.

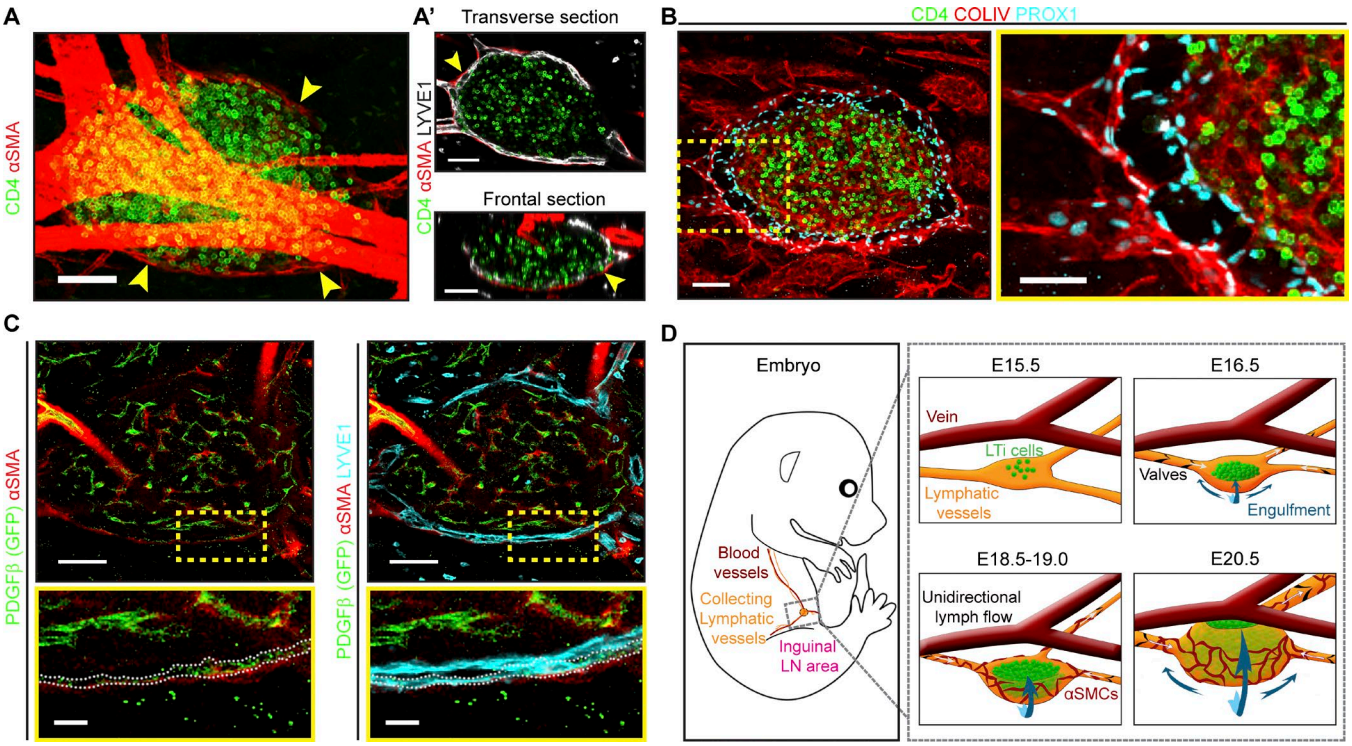

Figure 2. **SMC recruitment and deposition of basement membrane during LN capsule formation. (A)** SMCs surround iLN. Whole mount: αSMA (red) and CD4 (green). Arrowheads indicate LN SMCs. E18.5, *n* = 3. Scale bar, 50 µm. **(A')** Transverse and frontal views (1 µm) of A, LYVE1 (white). Scale bar, 50 µm. **(B)** Extracellular matrix deposition around iLN. Whole mount 10-µm transverse view: collagen IV (red), PROX1 (blue), and CD4 (green). High-magnification image is shown on the right. E18.5, *n* = 3. Scale bars, 50 µm and 30 µm. **(C)** LN LECs in contact with SMCs express PDGFβ. Whole mount of iLN from *Pdgfβ*-CreERT2-IRES-EGFP mice (1 µm): GFP (green), αSMA (red), and LYVE1 (blue). High-magnification images are shown at the bottom. Dotted line indicates PDGFβ$^+$ LYVE1$^+$ LECs. E18.5, *n* = 5. Scale bars, 100 µm and 20 µm. **(D)** LN capsule expansion steps. Artery and blood capillaries inside the LN are not shown.

represent sinus-traversing strands of adult LN SCS (Ohtani et al., 2003; Rantakari et al., 2015) and may be preventing the SCS lumen collapse, in addition to their role in filtering the afferent lymph. Finally, the CD169$^+$ macrophages inserted into the adult SCS fLEC layer prevent dissemination of pathogens and deliver antigens to adjacent B cells (Carrasco and Batista, 2007; Junt et al., 2007; Phan et al., 2007). Surprisingly, we observed CD169$^+$ macrophages within the fLEC layer already at E18.5 (Fig. 5 F). Taken together, our data show that specialization of SCS LECs is established prenatally, and this timing coincides with initiation of collecting lymphatic vessel maturation.

Disruption of collecting vessel specialization prevents LN capsule and SCS formation

We asked next whether disruption of collecting vessel specialization affects LN development. In *Foxc2*$^{-/-}$ mice, primary lymphatic capillary plexus fails to remodel into collecting vessels (Petrova et al., 2004; Norrmén et al., 2009). We analyzed LN development in *Foxc2*$^{f/f}$; *Prox1*-CreERT2 (*Foxc2*^{lecKO}) mice with LEC-specific loss of FOXC2. As described earlier (Sabine et al., 2015), *Foxc2*^{lecKO} embryos had a complete arrest of collecting vessel development, as determined by the absence of valves and expression of capillary markers LYVE1 and CCL21 in all LECs (Fig. 6 A and Fig. S3 B). In parallel with the failed collecting vessel maturation, formation of the LN capsule was severely disrupted: instead of a continuous lymphatic cup, *Foxc2*^{lecKO} iLN anlage was surrounded by a mesh-like vasculature, only partially enclosing the LN (Fig. 6 B).

The LN LECs in *Foxc2*^{lecKO} mice failed to express SCS LEC markers ITGA2B or CCRL1, whereas LYVE1 and MAdCAM1 were uniformly high. Moreover, mislocalized SMCs encircled the LN lymphatic vessels (Fig. 6, C–F'). Furthermore, while CD169$^+$ macrophages were aligned with fLECs in the WT iLN, in *Foxc2*^{lecKO} mice the number of macrophages was reduced, and they were dispersed throughout the LN (Fig. 6 G). These results demonstrate that FOXC2 ensures both collecting vessel maturation and prenatal LN LEC capsule specialization.

Impaired LN expansion, lymphatic trafficking of LTi cells, and CXCL13 expression in Foxc2^{lecKO} mice

From E18.5 onward, the *Foxc2*^{lecKO} iLNs were significantly smaller than controls (Fig. 7 A). Organization of axillary and mesenteric LNs was also perturbed, but the formation of nonencapsulated Peyer's patches was not affected (Fig. 7, B–F). We next investigated the reason for the reduced *Foxc2*^{lecKO} LN size. The LTi cells in both E18.5 control and *Foxc2*^{lecKO} animals were mostly quiescent, and staining for activated caspase 3 did not reveal differences in cell death (Fig. S3, C–E). Instead, we observed accumulation of intra- and extravascular CD4$^+$ cells and large intralymphatic clusters both in the vicinity of LN anlagen and throughout the dermal and mesenteric lymphatic vessels of *Foxc2*^{lecKO} mice (Fig. 7, G–K; and Fig. S3 F). These results demonstrate that collecting vessel mat-

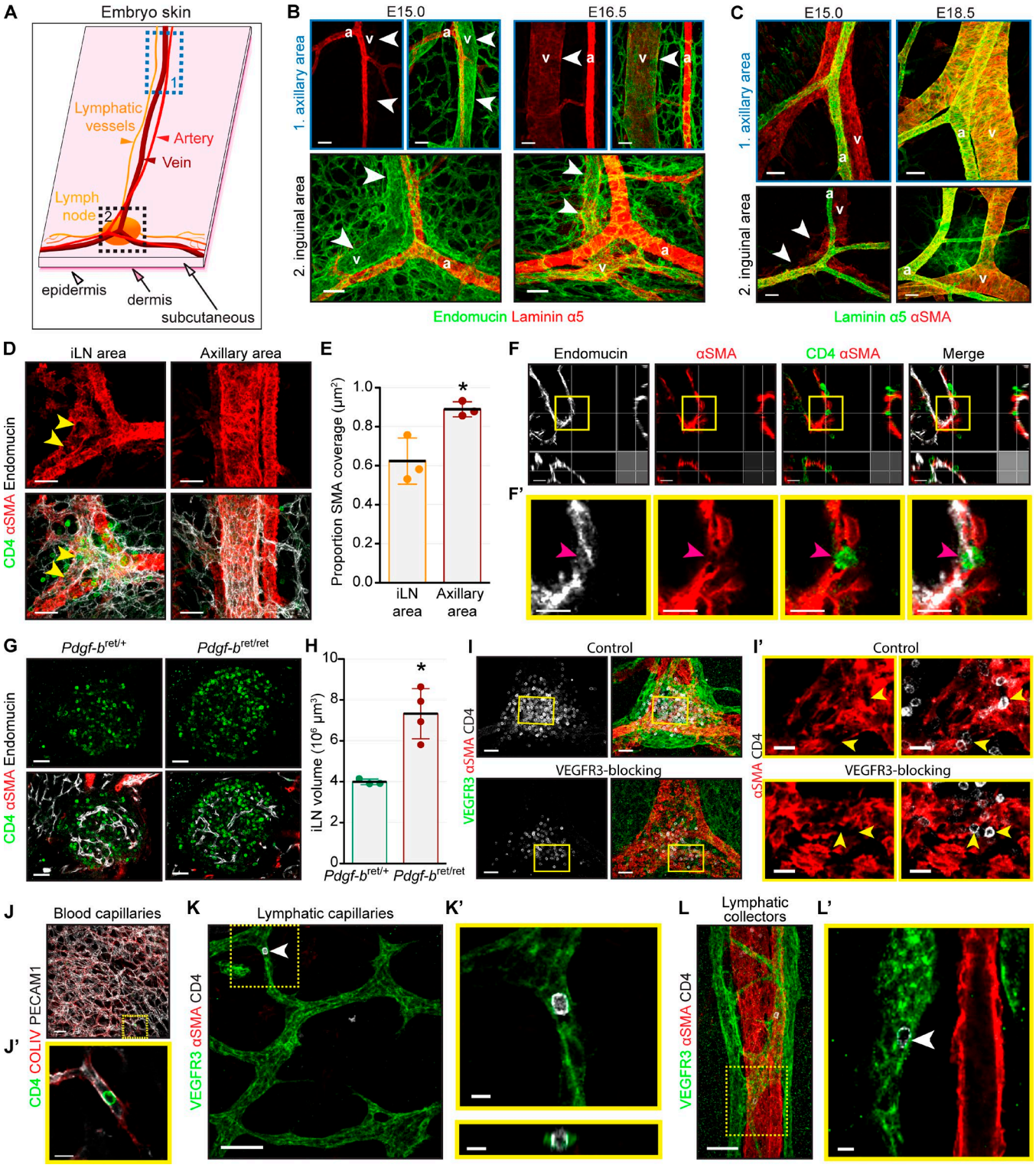

Figure 3. **Blood and lymphatic vessels contribute to early LN development. (A)** Skin areas analyzed. 1, axillary area; 2, inguinal area. **(B)** Laminin α5 is not produced by veins at E15.0. Whole mount: endomucin (green) and laminin α5 (red). v, vein; a, artery. Arrowheads indicate vein. E15.0, $n = 4$; E16.5, $n = 3$. Scale bar, 50 µm. **(C)** Differential venous SMC coverage in axillary versus inguinal areas at E15.0 but not at E18.5. Whole mount: αSMA (red) and laminin α5 (green). v, vein; a, artery. Arrowheads indicate SMC gaps on the vein. Scale bar, 50 µm. E15.0, $n = 5$; E18.5, $n = 3$. **(D)** Low venous SMC coverage in E15.0 iLN region. Whole mount: CD4 (green), αSMA (red), and endomucin (white). Arrowheads indicate SMC-low gaps. E15.0, $n = 3$. Scale bar, 50 µm. **(E)** Quantification of venous SMC coverage in iLN versus axillary area. E15.0, $n = 3$. *, $P < 0.05$. **(F)** LTi cells in αSMA-low areas. Whole mount of subepigastric vein (1 µm): CD4 (green), αSMA (red), and endomucin (white). **(F')** High magnification of F. Arrowhead indicates LTi cell in SMC-low space. E15.0, $n = 3$. Scale bars, 20 µm and 15 µm. **(G)** Increased LN size in *Pdgfb*$^{ret/ret}$ embryos. Whole mount iLN (1 µm): CD4 (green), endomucin (white), and αSMA (red). Scale bar, 50 µm. **(H)** Quantification of E17.5 *Pdgfb*$^{ret/+}$ and *Pdgfb*$^{ret/ret}$ iLN volume. *Pdgfb*$^{ret/+}$, $n = 3$; *Pdgfb*$^{ret/ret}$, $n = 4$. *, $P < 0.05$. **(I)** iLN anlagen of embryos treated with control or VEGFR3-blocking antibody. Whole mount iLN: VEGFR3 (green), αSMA (red), and CD4 (white). E15.5, $n = 4$ per treatment. Scale bar, 50 µm. **(I')** High-magnification view of I (1 µm). Arrowheads

uration is essential for LN capsule formation, SCS specialization, and further LN expansion.

Because of intralymphatic accumulation of LTi cell clusters in both *Cxcr5*$^{-/-}$ and *Foxc2*$^{\text{lecKO}}$ mice, we compared the expression of CXCR5 ligand *Cxcl13* as well as of *Ccl21* and *Ccl19* chemokines in *Foxc2*$^{\text{lecKO}}$ or WT iLNs. WT iLNs produced more *Cxcl13*, *Ccl21*, and *Ccl19* mRNA in comparison to the skin, and only *Cxcl13* mRNA was significantly decreased in the absence of FOXC2 (Fig. 8, A and B). On the protein level, CXCL13 but not VCAM1, ICAM1, and RANKL was reduced in *Foxc2*$^{\text{lecKO}}$ iLNs (Fig. 8, C–J). Because lower CXCL13 could be a result of reduced LTi cell number in *Foxc2*$^{\text{lecKO}}$ iLNs, we quantified CXCL13 and VCAM1 levels in E17.5 WT and E18.5 *Foxc2*$^{\text{lecKO}}$ iLNs, which have similar sizes (Fig. 8 K). Only CXCL13 but not VCAM1 was decreased in E17.5 *Foxc2*$^{\text{lecKO}}$ iLNs (Fig. 8, L–O), demonstrating that LTi cell number is not a critical parameter at this stage. These results show that lymphatic vessel specialization is important for stromal CXCL13 expression and LN expansion.

Interstitial fluid flow (IFF) potentiates production of Cxcl13 by fibroblasts

LTβR signaling promotes CXCL13 expression by fibroblastic LTo cells (Rennert et al., 1998; Dejardin et al., 2002; Müller and Siebenlist, 2003). However, LTβR, LTβ, or LTα expression was not affected in *Foxc2*$^{\text{lecKO}}$ iLNs (Fig. 8 B). We then reasoned that LTβR signaling, supplied by LTαβ^{+} LTi cells (Vondenhoff et al., 2009a), may be necessary but not sufficient to fully activate *Cxcl13* expression in LTo cells.

To clarify the mechanism of *Cxcl13* down-regulation in the *Foxc2*$^{\text{lecKO}}$ iLNs, we first asked whether LECs enhance CXCL13 production by LTo cells. We cultured mouse embryonic fibroblasts (MEFs) with LN LECs or LN LEC–conditioned medium in the presence or in the absence of LTβR-activating antibody (Fig. S4, A–C). As expected (Dejardin et al., 2002; Müller and Siebenlist, 2003), LTβR activation induced *Cxcl13* and *Vcam1* in MEFs (Fig. S4 C). However, co-culture with LECs or with LEC-conditioned medium suppressed the induction of *Cxcl13* (Fig. S4 C). Thus, direct contact with LECs is unlikely to induce *Cxcl13* in LTo cells.

By absorbing plasma leaking from blood capillaries, lymphatic vessels generate IFF, which has important morphogenetic functions (Starling, 1896; Wiig and Swartz, 2012). We reasoned that engulfment of LN anlagen by growing LN capsule creates high IFF, from the moment when embryonic maturing lymphatics initiate directional lymph transport. To analyze whether IFF affects *Cxcl13* expression in vitro, we cultured MEFs in three dimensions in the presence or absence of LTβR-activating antibody in static or IFF conditions (Fig. 9 A). As expected (Chambliss et al., 2013), IFF induced formation of actin stress fibers indicating cytoskeleton reorganization (Fig. 9 B). Most importantly, IFF potentiated the production of *Cxcl13* mRNA in response to LTβR activation (Fig. 9 C). To study IFF in vivo, we microinjected FITC-dextran in the forelimb interstitium of E18.5 control or *Foxc2*$^{\text{lecKO}}$ embryos. WT lymphatic vessels readily drained the dye, but transport into lymphatic vessels of *Foxc2*$^{\text{lecKO}}$ mice was strongly reduced (Fig. 9, D and E). We suggest that in addition to their role in LTi cell transport, perinodal lymphatics promote IFF, which cooperates with LTβR signaling to induce CXCL13 in fibroblastic LTo cells and thereby enhances LTi cell retention in the LN anlage (Fig. 10).

Discussion

We report a high-resolution analysis of coordinated changes occurring during lymphatic vessel and LN development. Our results clarify blood and lymphatic vessel contribution to LN initiation and expansion, describe the process of LN capsule and SCS formation, and reveal the key role of collecting lymphatic vessels and their transport function in LN development.

Blood and lymphatic vessels in LN initiation and expansion

Together with the results of Vondenhoff et al. (2009b), our data show that initiation of LNs occurs independently of lymphatic vessels. We propose that similar to leukocyte extravasation in inflammation, CD4^{-} pre-LTi cells initially egress in specific venous locations with low SMC coverage, thus defining positioning of the future LN, and undergo local maturation into CD4^{+} LTi cells. Embryos with reduced SMC coverage develop larger LNs, indicating that immature blood vessels are a prerequisite for LTi cell entry into the future LN area. In agreement with Onder et al. (2017), we also show that lymphatic vessels transport the disseminated LTi cells and thus play a critical role in the expansion of early LNs. Our results unify the previous views and further suggest that venous SMC coverage status in part defines the site and the time of pre-LTi cell egress. Our static imaging approach has limitations: it remains possible that the observed venous trafficking of LTi cells in iLN anlage represents the reverse migration into blood vessels. However, we found only CD4^{-} RORγt^{+} intravenous LTi cells in the iLN area, which is in agreement with previous work (Mebius et al., 1997) that postulated the existence of extravascular maturation of LTi cells. Live imaging and characterization of extravascular versus intravascular LTi cells will be invaluable for further unraveling this fascinating process. Because development of different LNs is guided by distinct kinetics, similar high-resolution studies should also be extended to other LNs.

A lymphatic engulfment model for LN formation

Lymphatic vessels undergo striking remodeling during LN development. Similar to other lymphatic vascular beds, this process is VEGFC/VEGFR3-dependent (Lee and Koh, 2016; this study), but it differs from sprouting lymphangiogenesis

indicate LTi cells in SMC-low gaps of the vein at iLN site. Scale bar, 20 µm. **(J)** LTi cells in blood capillaries. Whole mount skin: CD4 (green), collagen IV (red), and PECAM1 (white). E15.0, *n* = 4. Scale bar, 50 µm. **(J')** High-magnification view of J (1 µm). Scale bar, 15 µm. **(K)** LTi cells in lymphatic capillaries. Whole mount skin: VEGFR3 (green), αSMA (red), and CD4 (white). Arrowhead indicates intralymphatic LTi cell. E15.5, *n* = 4. Scale bar, 70 µm. **(K')** High magnification of 1-µm transverse (top) and frontal (bottom) views of the area outlined in K. Scale bar, 10 µm. **(L)** LTi cells in collecting vessels. Whole mount of skin: VEGFR3 (green), αSMA (red), and CD4 (white). E15.5, *n* = 4. Scale bar, 70 µm. **(L')** High magnification of L (1 µm). Arrowhead indicates intralymphatic LTi cell. Scale bar, 10 µm. Data are shown as mean ± SD. All quantifications use two-tailed unpaired Student's *t* test.

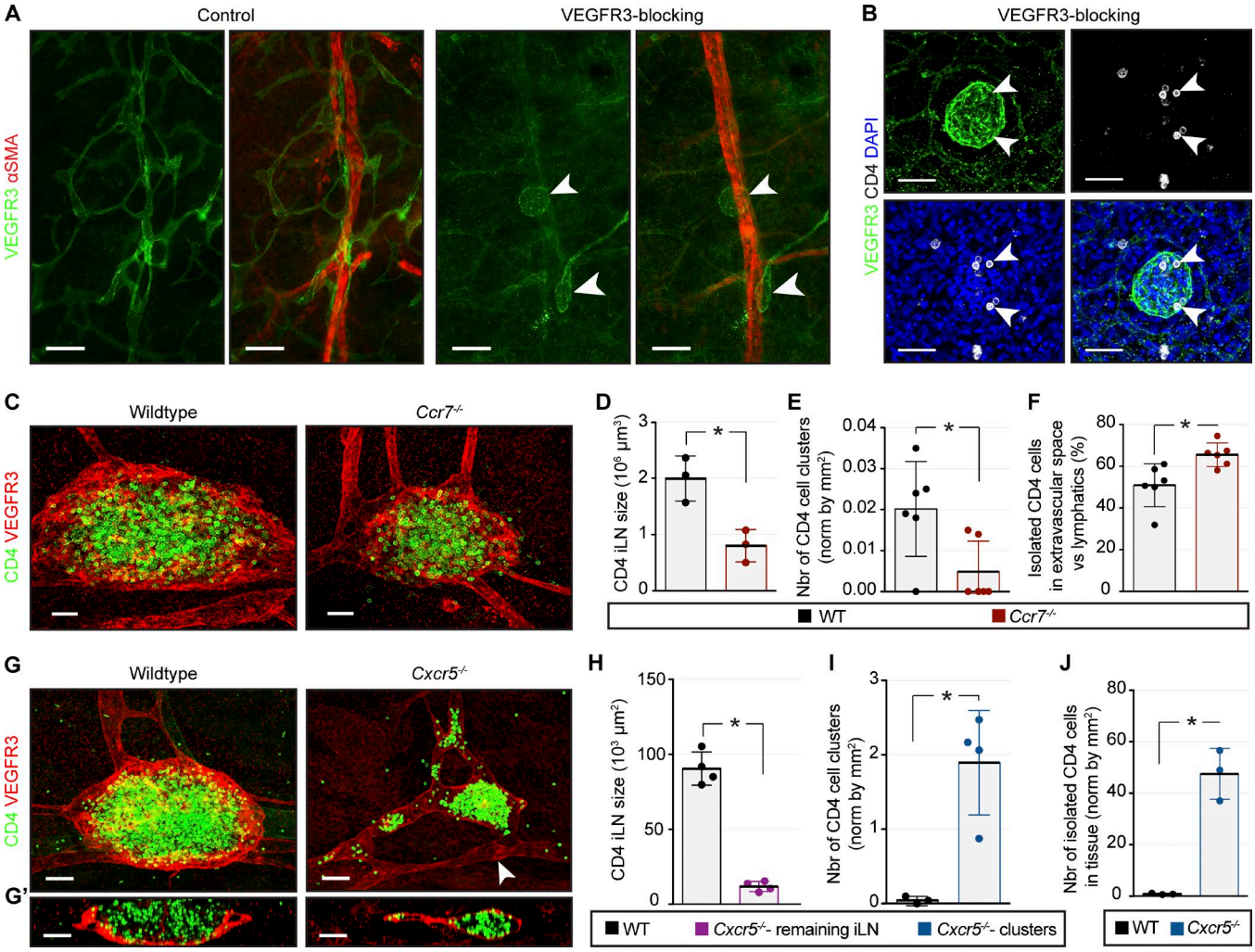

Figure 4. **Embryonic lymphatics transport LTi cells. (A)** LEC spheroids in embryos treated with VEGFR3-blocking antibody. Whole mount skin: VEGFR3 (green) and αSMA (red). Arrowheads indicate LEC spheroids. E15.5, *n* = 6 per treatment condition. Scale bar, 200 µm. **(B)** LTi cells in LEC spheroids. Whole mount skin: VEGFR3 (green), DAPI (blue), and CD4 (white). Arrowheads indicate intralymphatic LTi cells. E15.5, *n* = 6. Scale bar, 50 µm. **(C)** Smaller iLNs in *Ccr7*$^{-/-}$ embryos. Whole mount iLN: VEGFR3 (red) and CD4 (green). E18.5, *n* = 3 per genotype. Scale bar, 50 µm. **(D)** Quantification of iLN size in WT and *Ccr7*$^{-/-}$ embryos. E18.5, *n* = 3 per genotype; *, P < 0.05. **(E)** Quantification of intralymphatic CD4$^+$ clusters. E18.5, *n* = 6 per genotype; *, P < 0.05. **(F)** Percentage of extravascular CD4$^+$ cells in WT and *Ccr7*$^{-/-}$ skin. E18.5, *n* = 6 per genotype; *, P < 0.05. **(G)** Absence of cup-like lymphatic structures in *Cxcr5*$^{-/-}$ embryos. Whole mount iLN: VEGFR3 (red) and CD4 (green). **(G')** 10-µm frontal section. Arrowhead indicates lymphatic valve. E19.0, *n* = 3 per genotype. Scale bar, 50 µm. **(H)** CD4$^+$ inguinal cluster size in WT and *Cxcr5*$^{-/-}$ mice. E19.0, *n* = 4 per genotype; *, P < 0.05. **(I)** Quantification of intralymphatic CD4$^+$ clusters in WT and *Cxcr5*$^{-/-}$ E19.0 skin. WT, *n* = 3; *Cxcr5*$^{-/-}$, *n* = 4; *, P < 0.05. **(J)** Quantification of isolated CD4$^+$ cells in WT and *Cxcr5*$^{-/-}$ E19.0 skin. *n* = 3 per genotype; *, P < 0.05. Data are shown as mean ± SD. All quantifications use two-tailed unpaired Student's *t* test.

observed in peripheral lymphatics. The canonical lymphangiogenic response includes selection of tip cells, sprouting in response to a VEGFC gradient, followed by proliferation of stalk cells, which establish a vascular lumen and partially anastomose to form a mesh-like lymphatic vasculature (Ulvmar and Mäkinen, 2016). In contrast, collective migration and proliferation of LN LECs lead to formation of a double-walled cup-like structure, engulfing the developing LN, with only rare sprouting LECs observed at the top of converging EC sheets (Fig. 1 G). Why VEGFC induces LN engulfment rather than a sprouting response remains to be investigated. This could be due to the uniformly high production of VEGFC in LN cells, resulting in the absence of VEGFC gradient. Indeed, LTo cells express high VEGFC levels (Okuda et al., 2007), while LN LECs produce only low levels of the guidance molecule NRP2 that promotes VEGFC-driven LEC sprouting (Xu et al., 2010). Our results reveal the diversity of organ-specific mechanisms of lymphatic vessel expansion and highlight the need to further investigate the underlying mechanisms.

An advantage of LN engulfment versus lymphangiogenic sprouting is the maintenance of overall vessel integrity and transport function throughout the remodeling process, which is critical for bringing in the disseminated LTi cells. We also show that CCR7$^+$ LTi cells use CCL21$^+$ lymphatic capillaries as a direct route toward the LNs. However, albeit reduced in number, most LNs are present in mice lacking CCR7 or its ligands (Förster et al., 1999; Luther et al., 2003), indicating that additional mechanisms controlling lymphatic trafficking of LTi cells should exist.

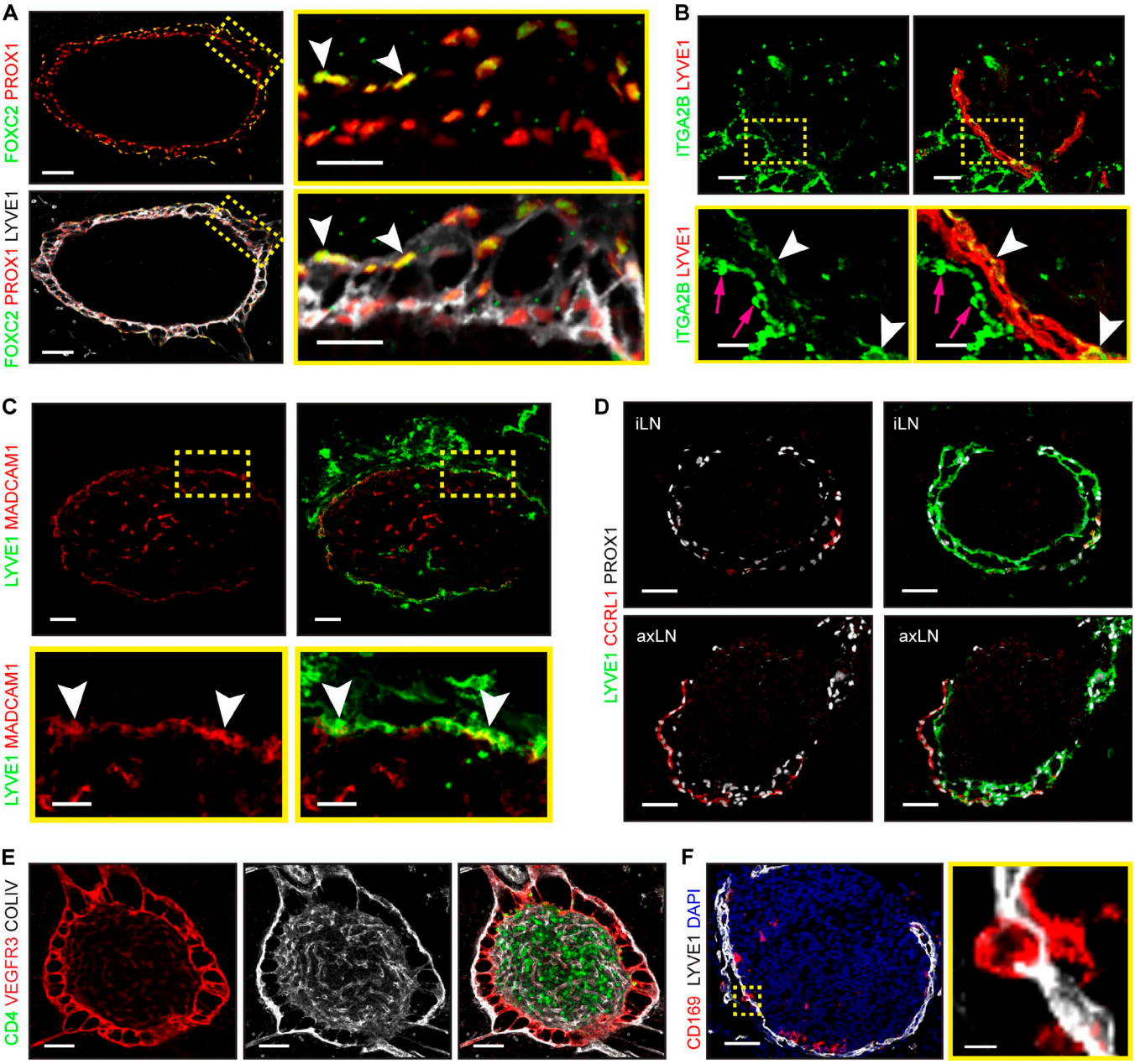

Figure 5. **Prenatal SCS LEC specification coincides with lymphatic vascular maturation. (A)** Collecting and capillary LEC markers in iLN lymphatics. Whole mount iLN (5-µm transverse section): FOXC2 (green), PROX1 (red), and LYVE1 (white). Arrowheads indicate PROX1$^+$/FOXC2$^+$ LECs. High-magnification images are shown on the right. E20.5, n = 1. The same expression pattern was observed at E16.5 (n = 3) and E18.5 (n = 1). Scale bars, 50 µm and 20 µm. **(B)** Staining of iLN for ITGA2B (green) and LYVE1 (red). High-magnification images are shown at the bottom. Arrowheads indicate ITGA2B$^+$ LECs; arrows indicate blood. E18.5, n = 3. Scale bars, 50 µm and 15 µm. **(C)** Staining of axLN for MADCAM1 (red) and LYVE1 (green). High-magnification images are shown at the bottom. Arrowheads indicate MADCAM1$^+$ LECs. E18.5–E20.5, n = 5. Scale bars, 50 µm and 20 µm. **(D)** Staining of E20.5 inguinal (iLN) and axillary (axLN) for CCRL1 (red), PROX1 (white), and LYVE1 (green). axLN, n = 4; iLN, n = 3. Scale bar, 50 µm. **(E)** LEC pillars connect two LN capsule layers. Whole mount (5-µm transverse section): collagen IV (white), VEGFR3 (red), and CD4 (green). E19.0, n = 3. Scale bar, 50 µm. **(F)** CD169$^+$ macrophages in the iLN SCS. Staining for CD169 (red), LYVE1 (white), and DAPI (blue). High-magnification image is shown on the right. E18.5–E20.5 iLN, n = 4. Scale bars, 50 µm and 5 µm.

LN SCS specialization and LN expansion are linked to collecting vessel formation

The adult LN SCS is lined by specialized LECs, which ensures optimal immune responses. The specification of SCS LECs occurs before birth and is characterized by acquisition of polarized expression of cLEC and fLEC markers CCRL1, ITGA2B, MADCAM1, and LYVE1; formation of transversal SCS LEC strands; recruitment of CD169$^+$ macrophages; and LN capsule SMCs (Fig. 5; Cordeiro et al., 2016). Thus, all cues for the differentiation of cLECs/fLECs and for positioning of specialized LN cells are present before birth. Importantly, we found that SCS specialization coincides with formation of collecting lymphatic vessels. By analyzing *Foxc2*$^{\text{lecKO}}$ embryos with defective collecting vessel morphogenesis we show that LN and collecting vessel development are highly coordinated, and disruption of collecting vessel function prevents formation of the LN capsule and SCS LEC specialization.

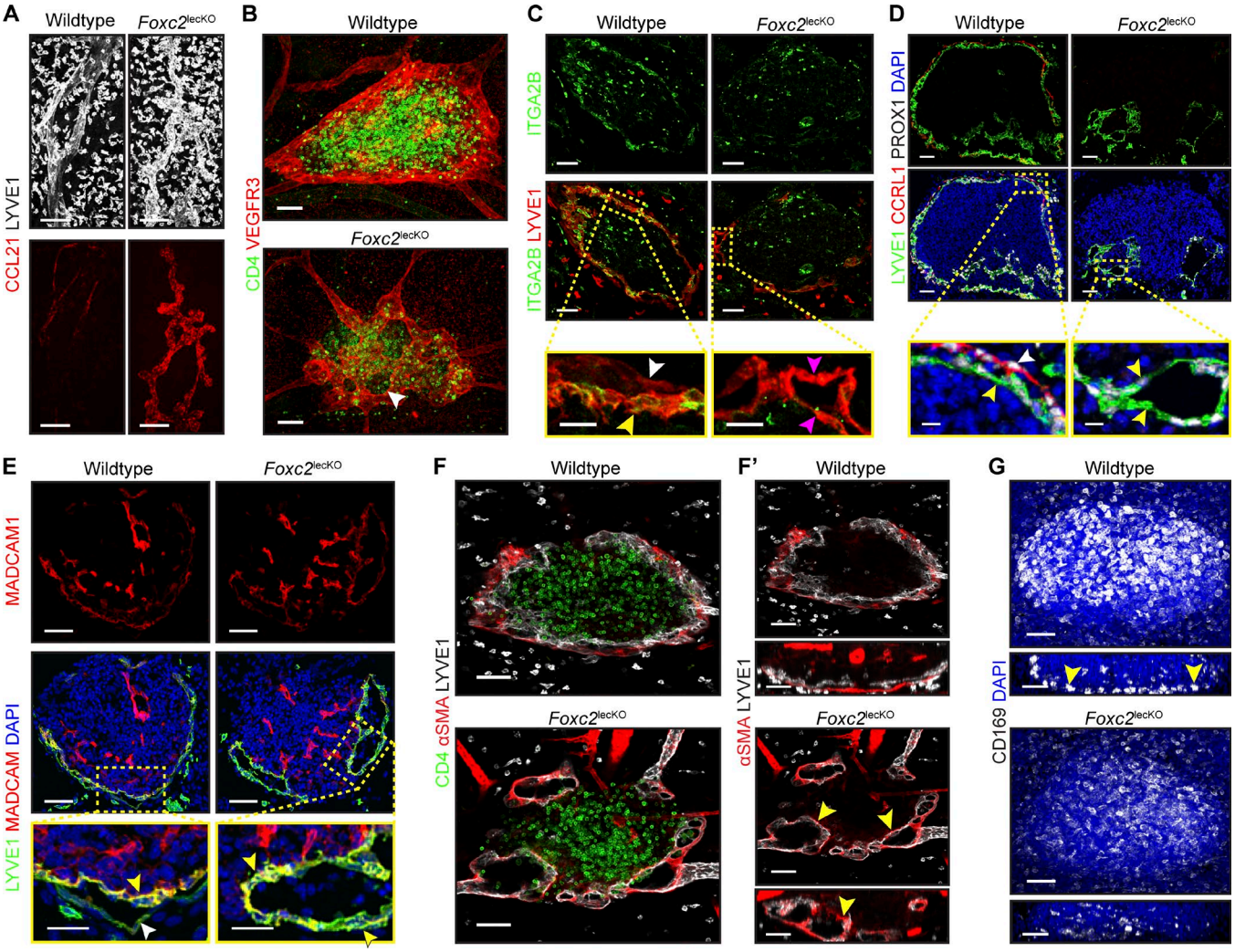

Figure 6. **Impaired collecting vessel development disrupts LN LEC specification and capsule formation. (A)** Increased LEC capillary markers in *Foxc2*^{lecKO} mice. Whole mount skin: CCL21 (red) and LYVE1 (white). Scale bar, 100 µm. E18.5, *n* = 2 per genotype. Similar expression pattern was observed at E20.5 (WT, *n* = 1; *Foxc2*^{lecKO}, *n* = 3). **(B)** Impaired LN capsule organization in *Foxc2*^{lecKO} embryos. Whole mount iLN area: CD4 (green) and VEGFR3 (red). Arrowhead indicates mesh-like lymphatic capsule. E19.0, *n* = 3 per genotype. Scale bar, 50 µm. **(C)** Loss of fLEC ITGA2B expression in *Foxc2*^{lecKO} mice. Staining of E18.5 iLN for ITGA2B (green) and LYVE1 (red). High-magnification images are shown at the bottom. White arrowhead indicates cLECs; yellow arrowhead indicates fLECs; pink arrowheads indicate *Foxc2*^{lecKO} unspecified LECs. WT, *n* = 3; *Foxc2*^{lecKO}, *n* = 5. Scale bars, 50 µm and 20 µm. **(D)** Reduced CCRL1 expression in *Foxc2*^{lecKO} LN. Staining of E20.5 axillary LN for LYVE1 (green), CCRL1 (red), PROX1 (white), and DAPI (blue). High-magnification images are shown at the bottom. White arrowhead indicates LYVE1^{low} CCRL1^{high} LECs; yellow arrowheads indicate LYVE1^{high} CCRL1^{neg} LECs. WT, *n* = 4; *Foxc2*^{lecKO}, *n* = 3. Scale bars, 50 µm and 10 µm. **(E)** Loss of polarized MADCAM1 in iLN LECs of *Foxc2*^{lecKO} mice. Staining for LYVE1 (green), MADCAM1 (red), and DAPI (blue). High-magnification images are shown at the bottom. White arrowhead indicates LYVE1^{low} MADCAM^{neg} LECs; yellow arrowheads indicate LYVE1^{high} MADCAM^{high} LECs. E18.5–E20.5 WT, *n* = 4; *Foxc2*^{lecKO}, *n* = 3. Scale bars, 50 µm and 25 µm. **(F)** Mislocalized SMC coverage on *Foxc2*^{lecKO} iLN lymphatics. Whole mount iLN (10 µm): CD4 (green), αSMA (red), and LYVE1 (white). **(F')** Transverse (top) and frontal (bottom) views (10 µm) of F. Arrowheads indicate ectopic SMCs. E18.5 WT, *n* = 3; *Foxc2*^{lecKO}, *n* = 4. Scale bar, 50 µm. **(G)** Reduced number and mislocalization of CD169^{+} macrophages in *Foxc2*^{lecKO} mice. Whole mount iLN: CD169 (white) and DAPI (blue). 10-µm frontal views are shown at the bottom. Arrowheads indicate CD169^{+} macrophages. E18.5–E19.0 WT, *n* = 5; *Foxc2*^{lecKO}, *n* = 4. Scale bar, 70 µm.

Role of biomechanical forces in LN development

CXCL13/CXCR5 signaling is indispensable for LTi cell retention within the LN anlagen and LN development (van de Pavert and Mebius, 2010). We show now that in *Cxcr5*$^{-/-}$ embryos, LTi cells are widely disseminated in the tissues and in the lymphatic vasculature. *Foxc2*^{lecKO} embryos display a similar phenotype indicating that functional collecting vessels participate in the regulation of CXCL13. Indeed, CXCL13 is selectively reduced in LTo cells of *Foxc2*^{lecKO} mice. Surprisingly, we found that the interstitial flow potentiates *Cxcl13* expression by LTβR-activated MEFs, and such flow is impaired in *Foxc2*^{lecKO} mice, indicating that lymphatic vessel transport function and IFF contribute to LN expansion. The expression of CCL21, induced by IFF in adult LN (Tomei et al., 2009), was not affected, suggesting a differential responsiveness of embryonic versus adult stromal cells. Primary cilia sense IFF (Nag and Resnick, 2017); however, loss of cilia did not affect IFF-dependent *Cxcl13* production by MEFs, indicating that alternative mechanisms are involved (unpublished data). How LTo cells sense IFF and how this process potentiates LTβR signaling at the molecular level will require more work. Most importantly,

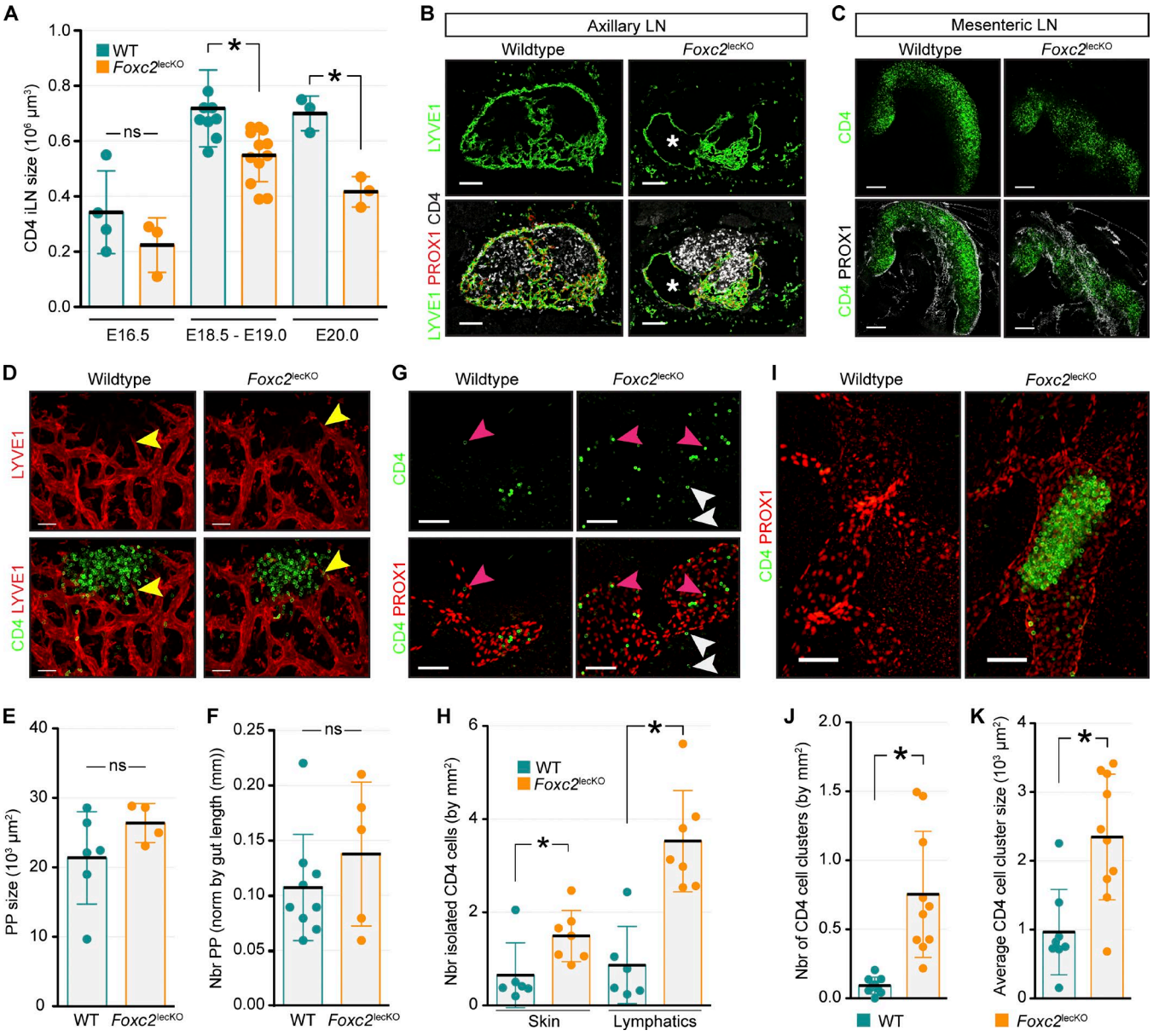

Figure 7. **Impaired LN expansion and trafficking of LTi cells in *Foxc2*^{lecKO} mice. (A)** iLN size in WT and *Foxc2*^{lecKO} embryos. E16.5, *n* = 4 and 3; E18.5–E19.0, *n* = 9 and 12; E20.0, *n* = 3 and 3 for WT and *Foxc2*^{lecKO} genotypes, respectively. *, P < 0.05. **(B)** Impaired axillary LN development in E20.5 *Foxc2*^{lecKO} embryos. Staining for LYVE1 (green), PROX1 (red), and CD4 (white). Asterisk indicates swollen LN lymphatics in *Foxc2*^{lecKO} mice. *n* = 2 per genotype. Scale bars, 100 µm. **(C)** Impaired mesenteric LN development in E18.5 *Foxc2*^{lecKO} embryos. Staining for CD4 (green) and PROX1 (white), 10-µm transverse sections. *n* = 4 per genotype. Scale bar, 200 µm. **(D)** Normal development of Peyer's patches (PPs) in E19.0 *Foxc2*^{lecKO} embryos. Whole mount staining for CD4 (green) and LYVE1 (red). Arrowheads indicate sprouting LECs. WT, *n* = 4; *Foxc2*^{lecKO}, *n* = 3. Scale bar, 50 µm. **(E)** Quantification of E18.5 PP size. WT, *n* = 6; *Foxc2*^{lecKO}, *n* = 4. **(F)** Quantification of E18.5 PP number. WT, *n* = 9; *Foxc2*^{lecKO}, *n* = 5. **(G)** Increased isolated CD4$^+$ LTi cells in *Foxc2*^{lecKO} dermis and lymphatic vessels. Whole mount E18.5 skin: CD4 (green) and PROX1 (red). Pink arrowheads indicate intralymphatic CD4 cells; white arrowheads indicate extravascular CD4 cells. WT, *n* = 3; *Foxc2*^{lecKO}, *n* = 4. Scale bar, 50 µm. **(H)** Quantification of isolated extralymphatic and intralymphatic CD4$^+$ cells in E18.5–E19.0 WT and *Foxc2*^{lecKO} embryos. WT, *n* = 6; *Foxc2*^{lecKO}, *n* = 7. *, P < 0.05. **(I)** Intralymphatic CD4$^+$ clusters in skin of *Foxc2*^{lecKO} embryo. Whole mount staining for CD4 (green) and PROX1 (red). E19.0 WT, *n* = 3; *Foxc2*^{lecKO}, *n* = 4. Scale bar, 50 µm. **(J)** Quantification of intralymphatic CD4$^+$ clusters in skin of E18.5–19.0 WT (*n* = 9) and *Foxc2*^{lecKO} (*n* = 10) mice. *, P < 0.05. **(K)** CD4$^+$ intralymphatic cluster size in E18.5–E19.0 skin of WT (*n* = 9) or *Foxc2*^{lecKO} (*n* = 10) embryos. *, P < 0.05. ns, not significant. Data are shown as mean ± SD. All quantifications use two-tailed unpaired Student's *t* test.

these results identify a new role of mechanical forces in LN development and suggest that IFF, generated by perinodal lymphatic vessels, enhances the efficiency of LTβR signaling between LTi and LTo cells and thus contributes to LN expansion.

In summary, our work reveals multiple roles of lymphatic vessels in LN development. While the initial LTi cell egress occurs from blood vessels, lymphatic vessels also participate in the LTi cell transport to LN anlagen. Around the LN anlage, collecting vessels reorganize into a capsule to further increase the efficiency of LTi cell delivery and retention. We further propose a novel role of IFF generated by perinodal lymphatics for potentiating CXCL13 expression by fibroblastic LTo cells in response to simultaneous LTβR signaling.

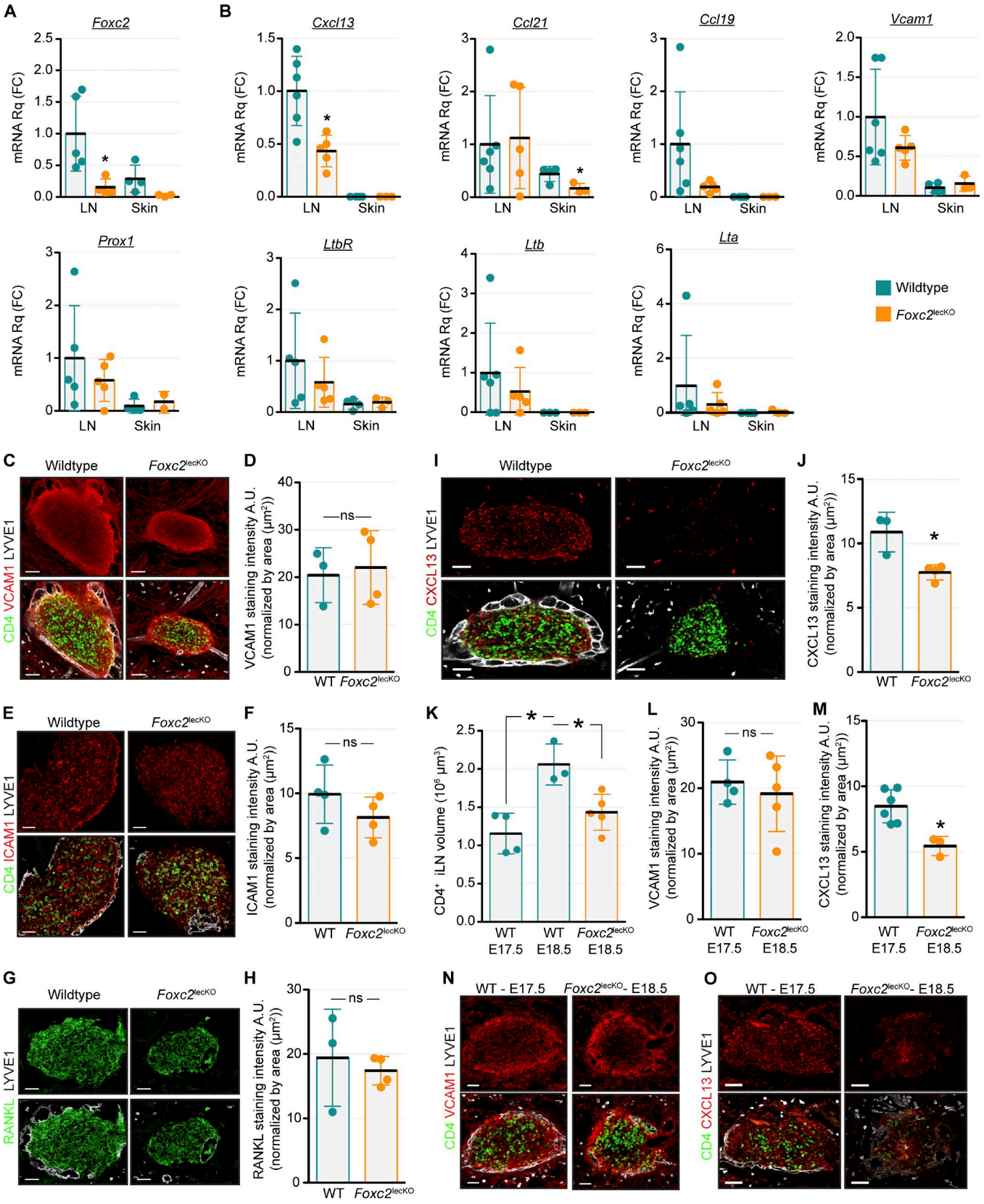

Figure 8. **Reduced *Cxcl13* in iLN of *Foxc2*^{lecKO} mice. (A and B)** Confirmation of *Foxc2* deletion at E18.5 in *Foxc2*^{lecKO} model (A) and *Cxcl13* mRNA selective reduction in E18.5 *Foxc2*^{lecKO} iLNs (B). RT-qPCR for the indicated genes in iLNs and skins. WT, n = 3–6; *Foxc2*^{lecKO}, n = 2–5. *, P < 0.05. **(C)** Comparable VCAM1 levels in E18.5 WT and *Foxc2*^{lecKO} embryos. Whole mount iLN (5 µm) for CD4 (green), VCAM1 (red), and LYVE1 (white). E18.5 WT, n = 3; *Foxc2*^{lecKO}, n = 4. Scale bar, 50 µm. **(D)** Quantification of VCAM1 intensity. E18.5 WT, n = 3; *Foxc2*^{lecKO}, n = 4. **(E)** Comparable levels of ICAM1 in WT and *Foxc2*^{lecKO} iLNs: CD4 (green), ICAM1 (red), and LYVE1 (white). E18.5–E20.5, n = 4 per genotype. Scale bar, 50 µm. **(F)** Quantification of ICAM1 intensity. E18.5–E20.5, n = 4 per genotype.

Materials and methods

Animal models

Animal experiments were approved by the Animal Ethics Committee of Canton of Vaud, Switzerland; by the Animal Experimentation Committee of the county of Münster, Germany; and by the Animal Experimentation Committee of Uppsala, Sweden. *Foxc2*$^{fl/fl}$ (Sabine et al., 2015), *Prox1*-Cre^{ERT2} (Bazigou et al., 2011), *Cxcr5*$^{-/-}$ (Förster et al., 1996), *Ltb*$^{-/-}$ (Koni et al., 1997), *Ccr7*$^{-/-}$ (Förster et al., 1999), *Pdgfb*^{ret} (Lindblom et al., 2003), *Id2*-Cre^{ERT2} (Rawlins et al., 2009), *Rorc*(γt)$^{EGFP/+}$ (Eberl et al., 2004), *Ccrl1*-eGFP (Heinzel et al., 2007), and *Pdgfβ*-CreERT2-IRES-EGFP (Claxton et al., 2008) were previously described. All mice were bred to at least the sixth generation on C57BL6/J background. For embryo experiments, matings were set up in the evening, and plugs were verified in the morning. Embryonic age (E) was determined according to the day of the vaginal plug (E0.5). For conditional gene inactivation, pregnant mice were injected with 5 mg of tamoxifen and 5 mg of progesterone in 100 µl sunflower seed oil between E13.5 and E14.5. When indicated, 5 µg/g EdU (Life Technologies) was injected i.p. 1 h before sacrifice. To block lymphangiogenesis, C57BL6/J pregnant mice were injected i.p. at E11.5 and E13.5 with 30 mg/kg rat anti-VEGFR3 (Pytowski et al., 2005) or control rat anti-HRPN IgG antibodies (BioXCell).

Microlymphangiography

Embryos were injected with 0.5–1 µl of 10 mg/ml 2,000-kD FITC-dextran (Sigma-Aldrich) into the interstitium of forelimb foot pads using a 10-µl Hamilton syringe. Lymphatic drainage was analyzed using Leica M205 FA stereomicroscope, Leica DFC 3000 G camera, and LAS X software.

Mouse tissue collection, staining procedures, and image acquisition

For whole mount staining, tissues were fixed with 4% paraformaldehyde (PFA), washed with PBS, permeabilized with 0.5% Triton X-100, and blocked with 5% donkey serum. Tissues were incubated with primary followed by secondary antibodies for 3 d on a rotating platform at 4°C and cleared using 3DISCO protocol (Ertürk et al., 2012) or alternatively incubated overnight with Histodenz (Sigma) at room temperature. 8-µm cryosections were 4% PFA–fixed, washed with PBS, permeabilized with 0.5% Triton-X-100, and blocked with 5% donkey serum. 5-µm deparaffinized tissue sections were subjected to heat-induced epitope retrieval (High pH Retrieval solution; DAKO). Click-it EdU Alexa Fluor 555 kit (Life Technologies) was used for EdU detection. For staining of cultured MEFs, cells were fixed with 4% PFA, washed with PBS, permeabilized with 0.1% Triton X-100, and blocked with 5% donkey serum. Alexa 488–conjugated phalloidin (Life Technologies) and DAPI (Sigma) were added to the chips overnight. Images were taken using confocal Zeiss LSM 880 or Leica SP5 Tandem microscopes and analyzed using Imaris and Adobe Photoshop software. Frontal stacks of whole mount images were on average 10 µm thick, and transverse stacks were 5–10 µm thick. Large image tiles were acquired using a motorized Zeiss Axio Observer.Z1 with AxioVision Rel.4.7 software. All frontal images of the embryonic iLN are shown with the epidermis facing downward. A list of antibodies used in this study is provided in Table S1.

Cell isolation and culture

MEFs from E14.5 embryos were prepared as described previously (González-Loyola et al., 2015) and cultured in complete DMEM. MEFs were used for experiments at passages 1–5. Mouse LN LECs were prepared as described (Dubrot et al., 2014), and LEC purity was confirmed by staining for LEC-specific PROX1 and EC-specific ERG. For co-culture experiments, MEFs and LN LECs were mixed at 50% in complete αMEM medium, seeded on a 6-well plate coated with mixed bovine type I collagen (10 µg/ml; Corning) and human plasma fibronectin (10 µg/ml; Sigma), and cultured for 24 h. To study paracrine signaling, complete endothelial cell medium or conditioned medium from LECs was added to confluent MEFs. To activate lymphotoxin signaling, 2 µg/ml of LTβR (clone 4H8; Adipogen) or control antibodies (MOPC21 muIgG2a) were used.

Cell culture in microfluidic devices

Microfluidic devices were described in and cell seeding protocol was adapted from Kim et al. (2016). MEFs were resuspended in complete DMEM and fibrinogen solution (2.5 mg/ml) at a concentration of 10 million cells/ml and mixed with thrombin (1 U/ml; Sigma). The cell mix was injected in the left central channel, and all remaining channels were filled with fibrin (2.5 mg/ml). After fibrin gel polymerization, complete DMEM was loaded in the channels and the reservoirs. Devices were kept at 37°C in the incubator overnight. The following day, medium was replaced with complete DMEM supplemented with 2 µg/ml of LTβR (clones 4H8 or 3C8; Adipogen) or control antibodies (MOPC21 muIgG2a). To create a 2–3 µm/s interstitial flow across the central channels, a pressure gradient was applied by transferring the medium between the two channel compartments every 12 h. After 48 h, cells were used for RNA extraction or staining. Images were taken using inverted confocal Zeiss LSM 880 microscope.

(G) Comparable levels of RANKL in WT and *Foxc2*^{lecKO} E18.5 iLNs: RANKL (green) and LYVE1 (white). E18.5 WT, *n* = 3; *Foxc2*^{lecKO}, *n* = 4. Scale bar, 50 µm. **(H)** Quantification of RANKL intensity. E18.5 WT, *n* = 3; *Foxc2*^{lecKO}, *n* = 4. **(I)** Reduced CXCL13 levels in *Foxc2*^{lecKO} iLNs. Whole mount iLN (1 µm): CD4 (green), CXCL13 (red), and LYVE1 (white). E18.5 WT, *n* = 3; *Foxc2*^{lecKO}, *n* = 4. Scale bar, 50 µm. **(J)** Quantification of CXCL13 intensity. E18.5 WT, *n* = 3; *Foxc2*^{lecKO}, *n* = 4. *, P < 0.05. **(K)** Quantification of iLN volume in WT and *Foxc2*^{lecKO} embryos. E17.5 WT, *n* = 4; E18.5 WT, *n* = 3; E18.5 *Foxc2*^{lecKO}, *n* = 5. One-way ANOVA test with Tukey post hoc test; *, P < 0.05. **(L)** Quantification of VCAM1 intensity in E17.5 WT versus E18.5 *Foxc2*^{lecKO} iLNs. WT, *n* = 4; *Foxc2*^{lecKO}, *n* = 5. **(M)** Quantification of CXCL13 intensity in E17.5 WT versus E18.5 *Foxc2*^{lecKO} iLNs. WT, *n* = 6; *Foxc2*^{lecKO}, *n* = 3. *, P < 0.05. **(N)** Comparable VCAM1 levels in E17.5 WT and E18.5 *Foxc2*^{lecKO} iLNs. Whole mount iLN (5 µm): CD4 (green), VCAM1 (red), and LYVE1 (white). WT, *n* = 4; *Foxc2*^{lecKO}, *n* = 5. Scale bar, 50 µm. **(O)** Reduced CXCL13 levels in E18.5 *Foxc2*^{lecKO} compared with E17.5 WT iLN: CD4 (green), CXCL13 (red), and LYVE1 (white). WT, *n* = 6; *Foxc2*^{lecKO}, *n* = 3. Scale bar, 70 µm. ns, not significant. Data are shown as mean ± SD. All quantifications but K used two-tailed unpaired Student's *t* test.

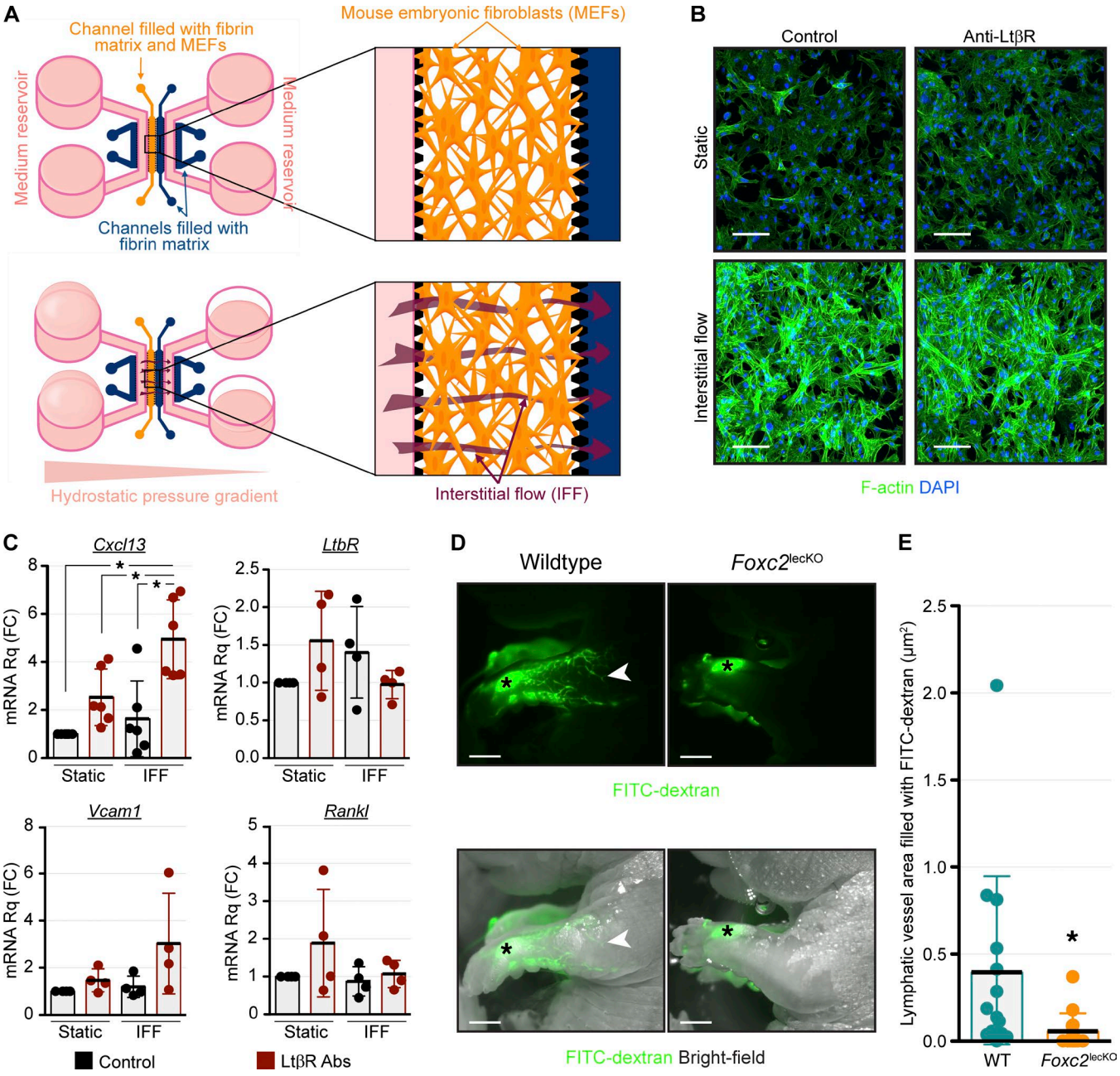

Figure 9. **IFF potentiates *Cxcl13* induction in response to LTβ signaling. (A)** MEFs were cultured in the left central channel of microfluidic device. Transfer of medium from one side to the other of the device creates a hydrostatic pressure gradient and IFF. **(B)** IFF induces actin stress fibers in MEFs: DAPI (blue) and F-actin (green). $n = 2$. Scale bar, 100 µm. **(C)** IFF potentiates *Cxcl13* expression in response to LTβ signaling. RT-qPCR analysis of the indicated genes after 48 h of IFF. *Cxcl13*, $n = 6$; *LtbR*, *Vcam1*, and *Rankl*, $n = 4$. One-way ANOVA test with Tukey post hoc test; *, $P < 0.05$. **(D)** Reduced interstitial FITC-dextran transport in E18.5 *Foxc2*^{lecKO} embryos. Arrowheads indicate FITC-dextran–filled lymphatics; asterisks indicate injection sites. Scale bar, 2.5 mm. **(E)** FITC-dextran lymphatic uptake in WT and *Foxc2*^{lecKO} mice. E18.5, $n = 14$ per genotype. Data are shown as mean ± SD. Two-tailed unpaired Student's *t* test; *, $P < 0.05$.

RNA extraction and real-time quantitative PCR (RT-qPCR)

iLNs or skins were dissected from E18.5 embryos and RNA isolated using the Qiagen RNeasy Plus Mini Kit (Qiagen). RNA was amplified using Ovation Pico WTA System V2 (Nugen). MEFs from chips and cells from co-culture experiments were collected using 0.05% trypsin-EDTA (Gibco) and RNA isolated using the Qiagen RNeasy Plus Micro or Mini Kit (Qiagen) and reverse transcribed using Transcriptor First Strand cDNA Synthesis Kit (Roche Diagnostics). We used StepOnePlus (Applied Biosystems) and SYBR Green PCR Master Mix (Applied Biosystems) or SensiFAST Sybr Hi-Rox Mix (Bioline) for qPCR analyses. Data were analyzed using the comparative Ct (ΔΔCt) method as described by the manufacturer. A list of primers used in this study is provided in Table S2.

Quantifications

Whole embryonic LNs were imaged using confocal Leica SP5 Tandem microscope. LN size was quantified using Imaris soft-

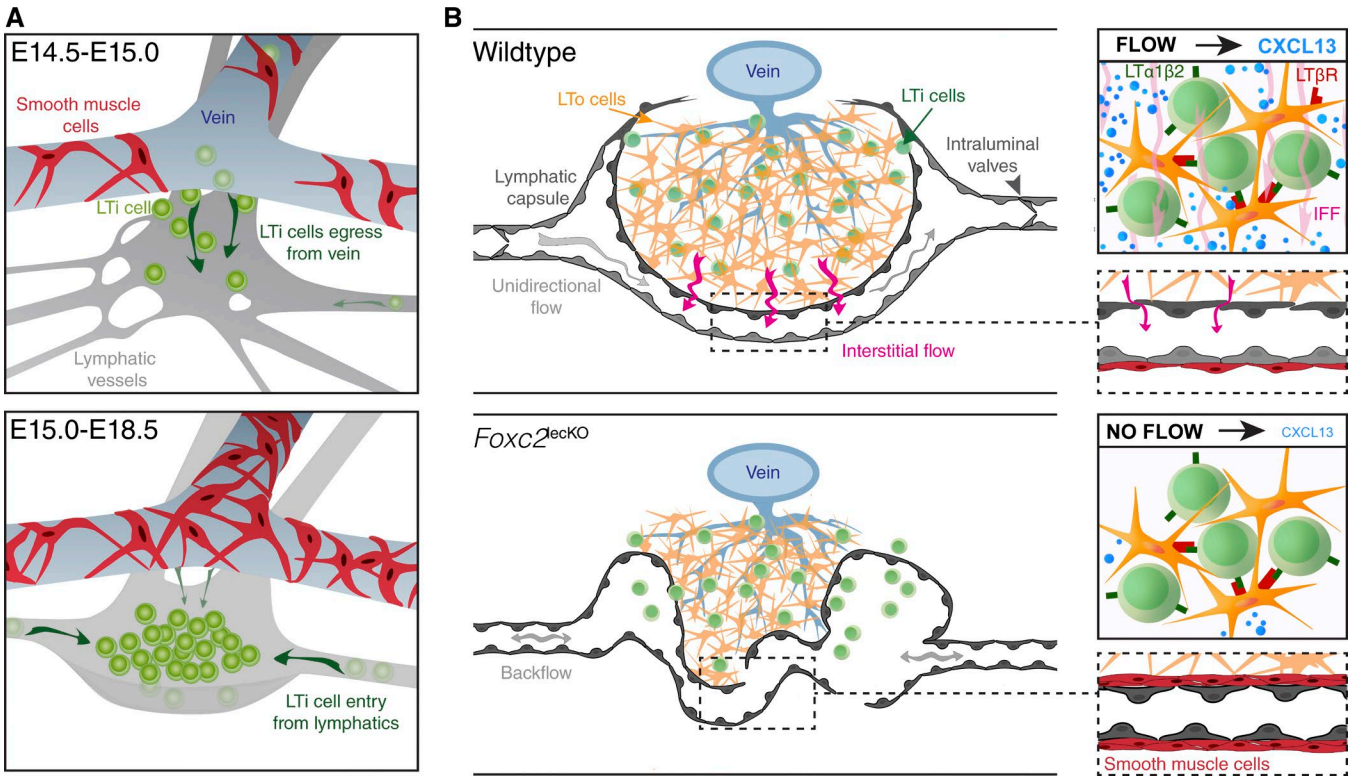

Figure 10. **Lymphatic vessels in LN development. (A)** LTi cells extravasate from the immature vein to initiate LN formation. At the same time, lymphatic vessels take up disseminated LTi cells, extravasating from blood capillaries elsewhere, and transport them to the LN anlage. Later, collecting vessels efficiently transport LTi cells to LNs and participate in their expansion. **(B)** Collecting vessels reorganize into a LN capsule, which engulfs the LN anlage. LN lymphatic fluid absorption from blood vessels generates IFF, which increases CXCL13 expression. Loss of *Foxc2* impairs LN capsule formation and leads to aberrant SMC coverage of LN lymphatic vessels precluding flow-induced CXCL13 production.

ware. Cell number in iLN area was quantified using Adobe Photoshop and ImageJ software. Skin tissue tiles were imaged with a motorized Zeiss Axio Observer.Z1. Skin intralymphatic clusters and isolated CD4$^+$ cells were manually analyzed and quantified using Adobe Photoshop and ImageJ software. To quantify the size and number of Peyer's patches, images were taken with a Leica DMI 3000 B microscope and Leica DFC 3000 G camera using LAS X software and analyzed using ImageJ software. For proliferation analyses, cells were double-stained for PROX1 and EdU. For every LN, whole LNs were analyzed in one transverse thick section (19.6 µm thick) at the top LN area and three thick sections homogenously distributed from the center of the LN (4.5 µm thick). Double PROX1 and EdU masks were applied using Imaris software, and cells were quantified using Adobe Photoshop and ImageJ software, counting as positive only cells in which all PROX1$^+$ area was EdU$^+$. False-positive cells due to partial overlap of PROX1$^+$ cells with adjacent proliferating EdU$^+$ cells were excluded. Activated caspase-3 intensity in CD4$^+$ area was quantified using Imaris software. For SMC coverage analysis, samples were stained for αSMA and endomucin. Double αSMA/endomucin masks were applied using Imaris software, and total endomucin and αSMA/endomucin area were quantified using Adobe Photoshop and ImageJ software. For all VCAM1 and CXCL13 protein-level analyses at E18.5, five Imaris-generated 4.5-µm-thick transverse sections per LN were analyzed using Adobe Photoshop and ImageJ. For CXCL13 in E17.5 WT and E18.5 *Foxc2*$^{\text{iecKO}}$ iLNs, ICAM1, and RANKL protein-level analyses, one cryosection per samples was analyzed using Adobe Photoshop and ImageJ. Staining intensity was quantified and normalized by the area analyzed. For FITC-draining experiments, FITC-filled lymphatic vessel area was quantified using Adobe Photoshop and ImageJ.

Statistics

Number of embryos analyzed is indicated for each image in the figure legends. For in vivo experiments comparing animals, we used a two-tailed unpaired Student's *t* test to determine statistical significance by calculating the probability of difference between two means. For iLN volume comparing E17.5 WT, E18.5 WT, and E18.5 *Foxc2*$^{\text{iecKO}}$ and for SMC coverage comparing *Id2*-Cre$^{\text{ERT2 tg/tg}}$ and *Id2*-Cre$^{\text{ERT2 tg/+}}$, we used one-way ANOVA with Tukey post hoc test. For in vitro experiments in microfluidic devices, we used a one-way ANOVA with Tukey post hoc test. Differences were considered statistically significant at $P < 0.05$. Data are shown as mean ± SD.

Online supplemental material

Fig. S1 provides further characterization of LTi cells and blood vascular maturation status during early iLN development. Fig. S2 provides characterization of intralymphatic CD4$^+$ LTi cells. Fig. S3 provides further characterization of lymphatic vessels in *Foxc2*$^{\text{iecKO}}$ mice. Fig. S4 shows that LECs reduce MEF expression

of CXCL13 in response to LTβR activation. Tables S1 and S2 provide information on antibodies and primers, respectively.

Acknowledgments

We thank L. Sorokin (University of Münster, Münster, Germany) for laminin α5 antibodies; A. Gonzalez Loyola for help with MEF isolation; T. Mäkinen (Uppsala University, Uppsala, Sweden), S. Hugues and J. Dubrot Armendariz (University of Geneva, Geneva, Switzerland), M. Fruttiger (University College London, London, UK), and P. Romero (University of Lausanne, Lausanne, Switzerland) for *Prox*1-CreERT2, *Rorc*(γt)$^{EGFP/+}$, *Pdgfβ*-CreERT2-IRES-EGFP, and *Id2*-Cre^{ERT2} mice, respectively; C. Beauverd for mouse genotyping and colony maintenance; A. Brendolan, J. Caamano, M. Dickinson, E. Lammert, J. Bernier-Latmani, and S. van de Pavert for useful discussions; and Animal, Cellular Imaging, Mouse Pathology and Genomic Technology Facilities of the University of Lausanne.

This work was supported by the Swiss National Science Foundation (31003A-156266 and 31ER30_160674 to T.V. Petrova), the Leenaards Foundation (to T.V. Petrova), Theodor and Gabriela Kummer and Société Académique Vaudoise fellowships (to E. Bovay), the Swedish Cancer Foundation (CAN2015/771 to C. Betsholtz), Vetenskapsrådet (VR2015-00550 to C. Betsholtz), Knut och Alice Wallenbergs Stiftelse (2012.0272 to C. Betsholtz), Fondation Leducq (14-CVD-02 to C. Olsson), the Deutsche Forschungsgemeinschaft (CRC656 and CRC1348 to F. Kiefer), and the National Research Foundation funded by the Ministry of Education of Korea (NRF-2018R1A2A1A05019550 to N.L. Jeon).

The authors declare no competing financial interests.

Author contributions: E. Bovay and T.V. Petrova conceived and designed research, interpreted the data, and drafted the manuscript; E. Bovay and B. Prat-Luri conducted experiments; E. Bovay acquired and analyzed data; A. Sabine, S. Luther, A.-H. Willrodt, C. Olsson, C. Halin, F. Kiefer, C. Betsholtz, S. Kim, K. Son, and N.L. Jeon provided reagents and intellectual input and interpreted the data; and all authors read, commented on, and approved the manuscript.

Submitted: 31 January 2018
Revised: 15 August 2018
Accepted: 4 October 2018

References

Ansel, K.M., V.N. Ngo, P.L. Hyman, S.A. Luther, R. Förster, J.D. Sedgwick, J.L. Browning, M. Lipp, and J.G. Cyster. 2000. A chemokine-driven positive feedback loop organizes lymphoid follicles. *Nature.* 406:309–314. https://doi.org/10.1038/35018581

Bazigou, E., O.T.A. Lyons, A. Smith, G.E. Venn, C. Cope, N.A. Brown, and T. Makinen. 2011. Genes regulating lymphangiogenesis control venous valve formation and maintenance in mice. *J. Clin. Invest.* 121:2984–2992. https://doi.org/10.1172/JCI58050

Brendolan, A., and J.H. Caamaño. 2012. Mesenchymal cell differentiation during lymph node organogenesis. *Front. Immunol.* 3:381. https://doi.org/10.3389/fimmu.2012.00381

Bromley, S.K., S.Y. Thomas, and A.D. Luster. 2005. Chemokine receptor CCR7 guides T cell exit from peripheral tissues and entry into afferent lymphatics. *Nat. Immunol.* 6:895–901. https://doi.org/10.1038/ni1240

Carrasco, Y.R., and F.D. Batista. 2007. B cells acquire particulate antigen in a macrophage-rich area at the boundary between the follicle and the subcapsular sinus of the lymph node. *Immunity.* 27:160–171. https://doi.org/10.1016/j.immuni.2007.06.007

Chambliss, A.B., S.B. Khatau, N. Erdenberger, D.K. Robinson, D. Hodzic, G.D. Longmore, and D. Wirtz. 2013. The LINC-anchored actin cap connects the extracellular milieu to the nucleus for ultrafast mechanotransduction. *Sci. Rep.* 3:1087. https://doi.org/10.1038/srep01087

Claxton, S., V. Kostourou, S. Jadeja, P. Chambon, K. Hodivala-Dilke, and M. Fruttiger. 2008. Efficient, inducible Cre-recombinase activation in vascular endothelium. *Genesis.* 46:74–80. https://doi.org/10.1002/dvg.20367

Cohen, J.N., C.J. Guidi, E.F. Tewalt, H. Qiao, S.J. Rouhani, A. Ruddell, A.G. Farr, K.S. Tung, and V.H. Engelhard. 2010. Lymph node-resident lymphatic endothelial cells mediate peripheral tolerance via Aire-independent direct antigen presentation. *J. Exp. Med.* 207:681–688. https://doi.org/10.1084/jem.20092465

Cordeiro, O.G., M. Chypre, N. Brouard, S. Rauber, F. Alloush, M. Romera-Hernandez, C. Bénézech, Z. Li, A. Eckly, M.C. Coles, et al. 2016. Integrin-Alpha IIb identifies murine lymph node lymphatic endothelial cells responsive to RANKL. *PLoS One.* 11:e0151848. https://doi.org/10.1371/journal.pone.0151848

Debes, G.F., C.N. Arnold, A.J. Young, S. Krautwald, M. Lipp, J.B. Hay, and E.C. Butcher. 2005. Chemokine receptor CCR7 required for T lymphocyte exit from peripheral tissues. *Nat. Immunol.* 6:889–894. https://doi.org/10.1038/ni1238

Dejardin, E., N.M. Droin, M. Delhase, E. Haas, Y. Cao, C. Makris, Z.-W. Li, M. Karin, C.F. Ware, and D.R. Green. 2002. The lymphotoxin-β receptor induces different patterns of gene expression via two NF-kappaB pathways. *Immunity.* 17:525–535. https://doi.org/10.1016/S1074-7613(02)00423-5

Dubrot, J., F.V. Duraes, L. Potin, F. Capotosti, D. Brighouse, T. Suter, S. Leibund-Gut-Landmann, N. Garbi, W. Reith, M.A. Swartz, and S. Hugues. 2014. Lymph node stromal cells acquire peptide-MHCII complexes from dendritic cells and induce antigen-specific CD4$^+$ T cell tolerance. *J. Exp. Med.* 211:1153–1166. https://doi.org/10.1084/jem.20132000

Eberl, G., S. Marmon, M.-J. Sunshine, P.D. Rennert, Y. Choi, and D.R. Littman. 2004. An essential function for the nuclear receptor RORgamma(t) in the generation of fetal lymphoid tissue inducer cells. *Nat. Immunol.* 5:64–73. https://doi.org/10.1038/ni1022

Ertürk, A., K. Becker, N. Jährling, C.P. Mauch, C.D. Hojer, J.G. Egen, F. Hellal, F. Bradke, M. Sheng, and H.-U. Dodt. 2012. Three-dimensional imaging of solvent-cleared organs using 3DISCO. *Nat. Protoc.* 7:1983–1995. https://doi.org/10.1038/nprot.2012.119

Escobedo, N., and G. Oliver. 2016. Lymphangiogenesis: Origin, specification, and cell fate determination. *Annu. Rev. Cell Dev. Biol.* 32:677–691. https://doi.org/10.1146/annurev-cellbio-111315-124944

Förster, R., A.E. Mattis, E. Kremmer, E. Wolf, G. Brem, and M. Lipp. 1996. A putative chemokine receptor, BLR1, directs B cell migration to defined lymphoid organs and specific anatomic compartments of the spleen. *Cell.* 87:1037–1047. https://doi.org/10.1016/S0092-8674(00)81798-5

Förster, R., A. Schubel, D. Breitfeld, E. Kremmer, I. Renner-Müller, E. Wolf, and M. Lipp. 1999. CCR7 coordinates the primary immune response by establishing functional microenvironments in secondary lymphoid organs. *Cell.* 99:23–33. https://doi.org/10.1016/S0092-8674(00)80059-8

González-Loyola, A., G. Fernández-Miranda, M. Trakala, D. Partida, K. Samejima, H. Ogawa, M. Cañamero, A. de Martino, Á. Martínez-Ramírez, G. de Cárcer, et al. 2015. Aurora B overexpression causes aneuploidy and p21Cip1 repression during tumor development. *Mol. Cell. Biol.* 35:3566–3578. https://doi.org/10.1128/MCB.01286-14

Heinzel, K., C. Benz, and C.C. Bleul. 2007. A silent chemokine receptor regulates steady-state leukocyte homing in vivo. *Proc. Natl. Acad. Sci. USA.* 104:8421–8426. https://doi.org/10.1073/pnas.0608274104

Honda, K., H. Nakano, H. Yoshida, S. Nishikawa, P. Rennert, K. Ikuta, M. Tamechika, K. Yamaguchi, T. Fukumoto, T. Chiba, and S.-I. Nishikawa. 2001. Molecular basis for hematopoietic/mesenchymal interaction during initiation of Peyer's patch organogenesis. *J. Exp. Med.* 193:621–630. https://doi.org/10.1084/jem.193.5.621

Junt, T., E.A. Moseman, M. Iannacone, S. Massberg, P.A. Lang, M. Boes, K. Fink, S.E. Henrickson, D.M. Shayakhmetov, N.C. Di Paolo, et al. 2007. Subcapsular sinus macrophages in lymph nodes clear lymph-borne viruses and present them to antiviral B cells. *Nature.* 450:110–114. https://doi.org/10.1038/nature06287

Kim, S., M. Chung, and N.L. Jeon. 2016. Three-dimensional biomimetic model to reconstitute sprouting lymphangiogenesis in vitro. *Biomaterials.* 78:115–128. https://doi.org/10.1016/j.biomaterials.2015.11.019

Koni, P.A., R. Sacca, P. Lawton, J.L. Browning, N.H. Ruddle, and R.A. Flavell. 1997. Distinct roles in lymphoid organogenesis for lymphotoxins α and β revealed in lymphotoxin β-deficient mice. *Immunity.* 6:491–500. https://doi.org/10.1016/S1074-7613(00)80292-7

Lee, Y.G., and G.Y. Koh. 2016. Coordinated lymphangiogenesis is critical in lymph node development and maturation. *Dev. Dyn.* 245:1189–1197. https://doi.org/10.1002/dvdy.24456

Lindblom, P., H. Gerhardt, S. Liebner, A. Abramsson, M. Enge, M. Hellström, G. Bäckström, S. Fredriksson, U. Landegren, H.C. Nyström, et al. 2003. Endothelial PDGF-B retention is required for proper investment of pericytes in the microvessel wall. *Genes Dev.* 17:1835–1840. https://doi.org/10.1101/gad.266803

Lund, A.W., F.V. Duraes, S. Hirosue, V.R. Raghavan, C. Nembrini, S.N. Thomas, A. Issa, S. Hugues, and M.A. Swartz. 2012. VEGF-C promotes immune tolerance in B16 melanomas and cross-presentation of tumor antigen by lymph node lymphatics. *Cell Reports.* 1:191–199. https://doi.org/10.1016/j.celrep.2012.01.005

Luther, S.A., K.M. Ansel, and J.G. Cyster. 2003. Overlapping roles of CXCL13, interleukin 7 receptor alpha, and CCR7 ligands in lymph node development. *J. Exp. Med.* 197:1191–1198. https://doi.org/10.1084/jem.20021294

Mäkinen, T., R.H. Adams, J. Bailey, Q. Lu, A. Ziemiecki, K. Alitalo, R. Klein, and G.A. Wilkinson. 2005. PDZ interaction site in ephrinB2 is required for the remodeling of lymphatic vasculature. *Genes Dev.* 19:397–410. https://doi.org/10.1101/gad.330105

Martinez-Corral, I., M.H. Ulvmar, L. Stanczuk, F. Tatin, K. Kizhatil, S.W.M. John, K. Alitalo, S. Ortega, and T. Makinen. 2015. Nonvenous origin of dermal lymphatic vasculature. *Circ. Res.* 116:1649–1654. https://doi.org/10.1161/CIRCRESAHA.116.306170

Mebius, R.E., P. Rennert, and I.L. Weissman. 1997. Developing lymph nodes collect CD4+CD3- LTbeta+ cells that can differentiate to APC, NK cells, and follicular cells but not T or B cells. *Immunity.* 7:493–504. https://doi.org/10.1016/S1074-7613(00)80371-4

Mebius, R.E., T. Miyamoto, J. Christensen, J. Domen, T. Cupedo, I.L. Weissman, and K. Akashi. 2001. The fetal liver counterpart of adult common lymphoid progenitors gives rise to all lymphoid lineages, CD45+CD4+CD3- cells, as well as macrophages. *J. Immunol.* 166:6593–6601. https://doi.org/10.4049/jimmunol.166.11.6593

Müller, J.R., and U. Siebenlist. 2003. Lymphotoxin β receptor induces sequential activation of distinct NF-κ B factors via separate signaling pathways. *J. Biol. Chem.* 278:12006–12012. https://doi.org/10.1074/jbc.M210768200

Nag, S., and A. Resnick. 2017. Biophysics and biofluid dynamics of primary cilia: evidence for and against the flow-sensing function. *Am. J. Physiol. Renal Physiol.* 313:F706–F720. https://doi.org/10.1152/ajprenal.00172.2017

Norrmén, C., K.I. Ivanov, J. Cheng, N. Zangger, M. Delorenzi, M. Jaquet, N. Miura, P. Puolakkainen, V. Horsley, J. Hu, et al. 2009. FOXC2 controls formation and maturation of lymphatic collecting vessels through cooperation with NFATc1. *J. Cell Biol.* 185:439–457. https://doi.org/10.1083/jcb.200901104

Ohl, L., G. Henning, S. Krautwald, M. Lipp, S. Hardtke, G. Bernhardt, O. Pabst, and R. Förster. 2003. Cooperating mechanisms of CXCR5 and CCR7 in development and organization of secondary lymphoid organs. *J. Exp. Med.* 197:1199–1204. https://doi.org/10.1084/jem.20030169

Ohl, L., M. Mohaupt, N. Czeloth, G. Hintzen, Z. Kiafard, J. Zwirner, T. Blankenstein, G. Henning, and R. Förster. 2004. CCR7 governs skin dendritic cell migration under inflammatory and steady-state conditions. *Immunity.* 21:279–288. https://doi.org/10.1016/j.immuni.2004.06.014

Ohtani, O., Y. Ohtani, C.J. Carati, and B.J. Gannon. 2003. Fluid and cellular pathways of rat lymph nodes in relation to lymphatic labyrinths and Aquaporin-1 expression. *Arch. Histol. Cytol.* 66:261–272. https://doi.org/10.1679/aohc.66.261

Okuda, M., A. Togawa, H. Wada, and S. Nishikawa. 2007. Distinct activities of stromal cells involved in the organogenesis of lymph nodes and Peyer's patches. *J. Immunol.* 179:804–811. https://doi.org/10.4049/jimmunol.179.2.804

Onder, L., U. Mörbe, N. Pikor, M. Novkovic, H.-W. Cheng, T. Hehlgans, K. Pfeffer, B. Becher, A. Waisman, T. Rülicke, et al. 2017. Lymphatic endothelial cells control initiation of lymph node organogenesis. *Immunity.* 47:80–92.e4. https://doi.org/10.1016/j.immuni.2017.05.008

Petrova, T.V., and G.Y. Koh. 2018. Organ-specific lymphatic vasculature: From development to pathophysiology. *J. Exp. Med.* 215:35–49. https://doi.org/10.1084/jem.20171868

Petrova, T.V., T. Karpanen, C. Norrmén, R. Mellor, T. Tamakoshi, D. Finegold, R. Ferrell, D. Kerjaschki, P. Mortimer, S. Ylä-Herttuala, et al. 2004. Defective valves and abnormal mural cell recruitment underlie lymphatic vascular failure in lymphedema distichiasis. *Nat. Med.* 10:974–981. https://doi.org/10.1038/nm1094

Phan, T.G., I. Grigorova, T. Okada, and J.G. Cyster. 2007. Subcapsular encounter and complement-dependent transport of immune complexes by lymph node B cells. *Nat. Immunol.* 8:992–1000. https://doi.org/10.1038/ni1494

Pytowski, B., J. Goldman, K. Persaud, Y. Wu, L. Witte, D.J. Hicklin, M. Skobe, K.C. Boardman, and M.A. Swartz. 2005. Complete and specific inhibition of adult lymphatic regeneration by a novel VEGFR-3 neutralizing antibody. *J. Natl. Cancer Inst.* 97:14–21. https://doi.org/10.1093/jnci/dji003

Rantakari, P., K. Auvinen, N. Jäppinen, M. Kapraali, J. Valtonen, M. Karikoski, H. Gerke, I. Iftakhar-E-Khuda, J. Keuschnigg, E. Umemoto, et al. 2015. The endothelial protein PLVAP in lymphatics controls the entry of lymphocytes and antigens into lymph nodes. *Nat. Immunol.* 16:386–396. https://doi.org/10.1038/ni.3101

Rawlins, E.L., C.P. Clark, Y. Xue, and B.L.M. Hogan. 2009. The Id2+ distal tip lung epithelium contains individual multipotent embryonic progenitor cells. *Development.* 136:3741–3745. https://doi.org/10.1242/dev.037317

Rennert, P.D., J.L. Browning, R. Mebius, F. Mackay, and P.S. Hochman. 1996. Surface lymphotoxin alpha/beta complex is required for the development of peripheral lymphoid organs. *J. Exp. Med.* 184:1999–2006. https://doi.org/10.1084/jem.184.5.1999

Rennert, P.D., D. James, F. Mackay, J.L. Browning, and P.S. Hochman. 1998. Lymph node genesis is induced by signaling through the lymphotoxin β receptor. *Immunity.* 9:71–79. https://doi.org/10.1016/S1074-7613(00)80589-0

Russo, E., A. Teijeira, K. Vaahtomeri, A.-H. Willrodt, J.S. Bloch, M. Nitschké, L. Santambrogio, D. Kerjaschki, M. Sixt, and C. Halin. 2016. Intralymphatic CCL21 promotes tissue egress of dendritic cells through afferent lymphatic vessels. *Cell Reports.* 14:1723–1734. https://doi.org/10.1016/j.celrep.2016.01.048

Sabine, A., Y. Agalarov, H. Maby-El Hajjami, M. Jaquet, R. Hägerling, C. Pollmann, D. Bebber, A. Pfenniger, N. Miura, O. Dormond, et al. 2012. Mechanotransduction, PROX1, and FOXC2 cooperate to control connexin37 and calcineurin during lymphatic-valve formation. *Dev. Cell.* 22:430–445. https://doi.org/10.1016/j.devcel.2011.12.020

Sabine, A., E. Bovay, C.S. Demir, W. Kimura, M. Jaquet, Y. Agalarov, N. Zangger, J.P. Scallan, W. Graber, E. Gulpinar, et al. 2015. FOXC2 and fluid shear stress stabilize postnatal lymphatic vasculature. *J. Clin. Invest.* 125:3861–3877. https://doi.org/10.1172/JCI80454

Schulte-Merker, S., A. Sabine, and T.V. Petrova. 2011. Lymphatic vascular morphogenesis in development, physiology, and disease. *J. Cell Biol.* 193:607–618. https://doi.org/10.1083/jcb.201012094

Starling, E.H. 1896. On the absorption of fluids from the connective tissue spaces. *J. Physiol.* 19:312–326. https://doi.org/10.1113/jphysiol.1896.sp000596

Tewalt, E.F., J.N. Cohen, S.J. Rouhani, C.J. Guidi, H. Qiao, S.P. Fahl, M.R. Conaway, T.P. Bender, K.S. Tung, A.T. Vella, et al. 2012. Lymphatic endothelial cells induce tolerance via PD-L1 and lack of costimulation leading to high-level PD-1 expression on CD8 T cells. *Blood.* 120:4772–4782. https://doi.org/10.1182/blood-2012-04-427013

Tomei, A.A., S. Siegert, M.R. Britschgi, S.A. Luther, and M.A. Swartz. 2009. Fluid flow regulates stromal cell organization and CCL21 expression in a tissue-engineered lymph node microenvironment. *J. Immunol.* 183:4273–4283. https://doi.org/10.4049/jimmunol.0900835

Ulvmar, M.H., and T. Mäkinen. 2016. Heterogeneity in the lymphatic vascular system and its origin. *Cardiovasc. Res.* 111:310–321. https://doi.org/10.1093/cvr/cvw175

Ulvmar, M.H., K. Werth, A. Braun, P. Kelay, E. Hub, K. Eller, L. Chan, B. Lucas, I. Novitzky-Basso, K. Nakamura, et al. 2014. The atypical chemokine receptor CCRL1 shapes functional CCL21 gradients in lymph nodes. *Nat. Immunol.* 15:623–630. https://doi.org/10.1038/ni.2889

van de Pavert, S.A., and R.E. Mebius. 2010. New insights into the development of lymphoid tissues. *Nat. Rev. Immunol.* 10:664–674. https://doi.org/10.1038/nri2832

van de Pavert, S.A., B.J. Olivier, G. Goverse, M.F. Vondenhoff, M. Greuter, P. Beke, K. Kusser, U.E. Höpken, M. Lipp, K. Niederreither, et al. 2009. Chemokine CXCL13 is essential for lymph node initiation and is induced by retinoic acid and neuronal stimulation. *Nat. Immunol.* 10:1193–1199. https://doi.org/10.1038/ni.1789

van de Pavert, S.A., M. Ferreira, R.G. Domingues, H. Ribeiro, R. Molenaar, L. Moreira-Santos, F.F. Almeida, S. Ibiza, I. Barbosa, G. Goverse, et al. 2014. Maternal retinoids control type 3 innate lymphoid cells and set the offspring immunity. *Nature.* 508:123–127. https://doi.org/10.1038/nature13158

Vondenhoff, M.F., M. Greuter, G. Goverse, D. Elewaut, P. Dewint, C.F. Ware, K. Hoorweg, G. Kraal, and R.E. Mebius. 2009a. LTbetaR signaling induces cytokine expression and up-regulates lymphangiogenic factors in lymph node anlagen. *J. Immunol.* 182:5439–5445. https://doi.org/10.4049/jimmunol.0801165

Vondenhoff, M.F., S.A. van de Pavert, M.E. Dillard, M. Greuter, G. Goverse, G. Oliver, and R.E. Mebius. 2009b. Lymph sacs are not required for the initiation of lymph node formation. *Development.* 136:29–34. https://doi.org/10.1242/dev.028456

Wang, Y., Y. Jin, M.A. Mäe, Y. Zhang, H. Ortsäter, C. Betsholtz, T. Mäkinen, and L. Jakobsson. 2017. Smooth muscle cell recruitment to lymphatic vessels requires PDGFB and impacts vessel size but not identity. *Development.* 144:3590–3601. https://doi.org/10.1242/dev.147967

Wiig, H., and M.A. Swartz. 2012. Interstitial fluid and lymph formation and transport: physiological regulation and roles in inflammation and cancer. *Physiol. Rev.* 92:1005–1060. https://doi.org/10.1152/physrev.00037.2011

Wu, C., F. Ivars, P. Anderson, R. Hallmann, D. Vestweber, P. Nilsson, H. Robenek, K. Tryggvason, J. Song, E. Korpos, et al. 2009. Endothelial basement membrane laminin α5 selectively inhibits T lymphocyte extravasation into the brain. *Nat. Med.* 15:519–527. https://doi.org/10.1038/nm.1957

Xu, Y., L. Yuan, J. Mak, L. Pardanaud, M. Caunt, I. Kasman, B. Larrivée, R. Del Toro, S. Suchting, A. Medvinsky, et al. 2010. Neuropilin-2 mediates VEGF-C-induced lymphatic sprouting together with VEGFR3. *J. Cell Biol.* 188:115–130. https://doi.org/10.1083/jcb.200903137

Yokota, Y., A. Mansouri, S. Mori, S. Sugawara, S. Adachi, S. Nishikawa, and P. Gruss. 1999. Development of peripheral lymphoid organs and natural killer cells depends on the helix-loop-helix inhibitor Id2. *Nature.* 397:702–706. https://doi.org/10.1038/17812

Yoshida, H., H. Kawamoto, S.M. Santee, H. Hashi, K. Honda, S. Nishikawa, C.F. Ware, Y. Katsura, and S.I. Nishikawa. 2001. Expression of alpha(4) beta(7) integrin defines a distinct pathway of lymphoid progenitors committed to T cells, fetal intestinal lymphotoxin producer, NK, and dendritic cells. *J. Immunol.* 167:2511–2521. https://doi.org/10.4049/jimmunol.167.5.2511

Zheng, W., H. Nurmi, S. Appak, A. Sabine, E. Bovay, E.A. Korhonen, F. Orsenigo, M. Lohela, G. D'Amico, T. Holopainen, et al. 2014. Angiopoietin 2 regulates the transformation and integrity of lymphatic endothelial cell junctions. *Genes Dev.* 28:1592–1603. https://doi.org/10.1101/gad.237677.114